Article

Cell Reports

Androgen Receptor Deregulation Drives Bromodomain-Mediated Chromatin Alterations in Prostate Cancer

Graphical Abstract

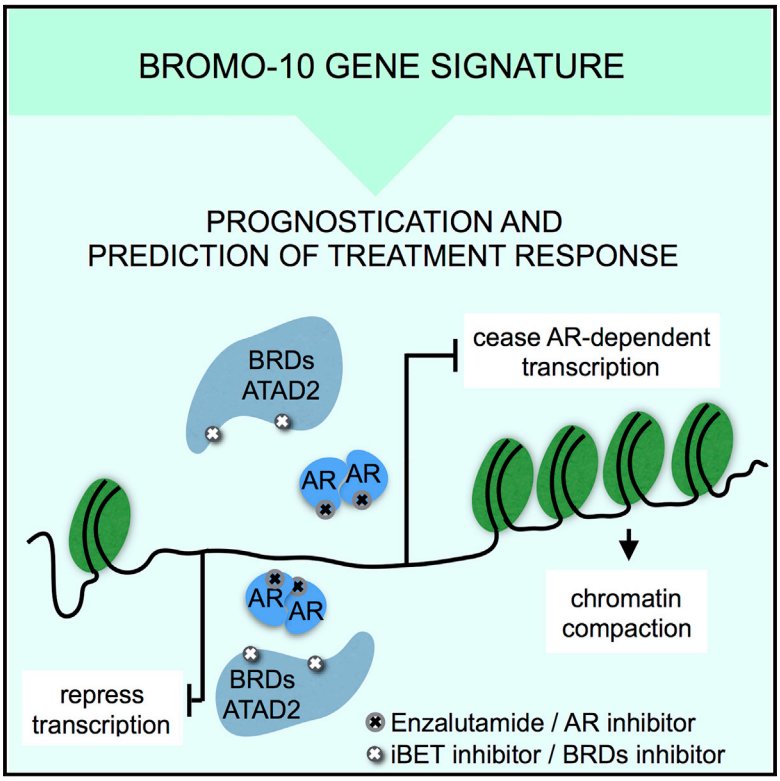

Highlights

- Androgen receptor (AR) overexpression drives genome-wide chromatin relaxation
- Bromodomain (BRD) inhibitors reduce local chromatin opening at AR target genes
- AR overexpression upregulates BRD proteins ATAD2, BRD2, and BRD4
- The BROMO-10 gene signature stratifies patients for therapy with BRD inhibitors

Authors

Alfonso Urbanucci, Stefan J. Barfeld, Ville Kytölä, ..., Matti Nykter, Tapio Visakorpi, Ian G. Mills

Correspondence

alfonsourbanucci@gmail.com (A.U.), i.g.mills@ncmm.uio.no (I.G.M.)

In Brief

Urbanucci et al. report how upregulated androgen receptor (AR) and AR-targeted bromodomain proteins contribute to genome-wide chromatin relaxation and increased gene transcription in advanced prostate cancer. They show that ATAD2 is a strong tissue biomarker and propose a BROMO-10 gene signature to stratify patients for combination therapies with bromodomain inhibitors.

Accession Numbers

GSE73989

Urbanucci et al., 2017, Cell Reports *19*, 2045–2059
June 6, 2017
http://dx.doi.org/10.1016/j.celrep.2017.05.049

Cell Reports
Article

Androgen Receptor Deregulation Drives Bromodomain-Mediated Chromatin Alterations in Prostate Cancer

Alfonso Urbanucci,[1,2,*] Stefan J. Barfeld,[1] Ville Kytölä,[3] Harri M. Itkonen,[1] Ilsa M. Coleman,[4] Daniel Vodák,[5] Liisa Sjöblom,[6] Xia Sheng,[7] Teemu Tolonen,[8] Sarah Minner,[9] Christoph Burdelski,[10] Kati K. Kivinummi,[3] Annika Kohvakka,[6] Steven Kregel,[11,12] Mandeep Takhar,[13] Mohammed Alshalalfa,[13] Elai Davicioni,[13] Nicholas Erho,[13] Paul Lloyd,[14,15] R. Jeffrey Karnes,[16] Ashley E. Ross,[17] Edward M. Schaeffer,[18] Donald J. Vander Griend,[11] Stefan Knapp,[19,20] Eva Corey,[21] Felix Y. Feng,[14,15,22] Peter S. Nelson,[4,21,23] Fahri Saatcioglu,[7,24] Karen E. Knudsen,[25] Teuvo L.J. Tammela,[26] Guido Sauter,[9] Thorsten Schlomm,[27] Matti Nykter,[3] Tapio Visakorpi,[6] and Ian G. Mills[1,2,28,29,*]

[1]Centre for Molecular Medicine Norway, Nordic European Molecular Biology Laboratory Partnership, Forskningsparken, University of Oslo, 21 0349 Oslo, Norway
[2]Department of Molecular Oncology, Institute for Cancer Research, Oslo University Hospital, 0424 Oslo, Norway
[3]Prostate Cancer Research Center, Institute of Biosciences and Medical Technology (BioMediTech), University of Tampere and Tampere University of Technology, 33520 Tampere, Finland
[4]Division of Human Biology, Fred Hutchinson Cancer Research Center, Seattle, WA 98109, USA
[5]Department of Tumor Biology, Institute for Cancer Research, The Norwegian Radium Hospital, Oslo University Hospital, 0424 Oslo, Norway
[6]Prostate Cancer Research Center, Institute of Biosciences and Medical Technology (BioMediTech), University of Tampere and Fimlab Laboratories, Tampere University Hospital, 33520 Tampere, Finland
[7]Department of Biosciences, University of Oslo, 0316 Oslo, Norway
[8]Department of Pathology, Fimlab Laboratories, Tampere University Hospital, 33520 Tampere, Finland
[9]University Medical Center Hamburg-Eppendorf, 20251 Hamburg, Germany
[10]General, Visceral and Thoracic Surgery Department and Clinic, University Medical Center Hamburg-Eppendorf, 20246 Hamburg, Germany
[11]Department of Surgery - Section of Urology, University of Chicago, Chicago, IL 60637, USA
[12]Michigan Center for Translational Pathology, University of Michigan, Ann Arbor, MI 48109-0940, USA
[13]Research and Development, GenomeDx Biosciences, Vancouver, BC V6B 1B8, Canada
[14]Department of Medicine, University of California at San Francisco, San Francisco, CA 94143-0410, USA
[15]Helen Diller Comprehensive Cancer Center, University of California, San Francisco, CA 94143-0981, USA
[16]Department of Urology, Mayo Clinic, Rochester, MN 55902, USA
[17]Brady Urological Institute, Johns Hopkins Medical Institute, Baltimore, MD 21287, USA
[18]Department of Urology, Northwestern University, Feinberg School of Medicine, 303 East Chicago Avenue, Tarry 16-703, Chicago, IL 60611-3008, USA
[19]Nuffield Department of Clinical Medicine, University of Oxford, Old Road Campus, Roosevelt Drive, Oxford OX3 7DQ, UK
[20]Institute for Pharmaceutical Chemistry, Goethe-University Frankfurt, Campus Riedberg, Max-von Laue Strasse 9, 60438 Frankfurt am Main, Germany
[21]Department of Urology, University of Washington, Seattle, WA 98195, USA
[22]Department of Radiation Oncology, University of California, San Francisco, San Francisco, CA 94115, USA
[23]Department of Pathology, University of Washington, Seattle, WA 98195, USA
[24]Institute for Cancer Genetics and Informatics, Oslo University Hospital, 0424 Oslo, Norway
[25]Sidney Kimmel Cancer Center, Thomas Jefferson University, Philadelphia, PA 19107, USA
[26]Prostate Cancer Research Center and Department of Urology, University of Tampere and Tampere University Hospital, 33014 Tampere, Finland
[27]Martini-Clinic, Prostate Cancer Center, University Medical Center Hamburg-Eppendorf, Hamburg 20095, Germany
[28]PCUK Movember Centre of Excellence, CCRCB, Queen's University, Belfast BT7 1NN, Northern Ireland, UK
[29]Lead Contact
*Correspondence: alfonsourbanucci@gmail.com (A.U.), i.g.mills@ncmm.uio.no (I.G.M.)
http://dx.doi.org/10.1016/j.celrep.2017.05.049

SUMMARY

Global changes in chromatin accessibility may drive cancer progression by reprogramming transcription factor (TF) binding. In addition, histone acetylation readers such as bromodomain-containing protein 4 (BRD4) have been shown to associate with these TFs and contribute to aggressive cancers including prostate cancer (PC). Here, we show that chromatin accessibility defines castration-resistant prostate cancer (CRPC). We show that the deregulation of androgen receptor (AR) expression is a driver of chromatin relaxation and that AR/androgen-regulated bromodomain-containing proteins (BRDs) mediate this effect. We also report that BRDs are overexpressed in CRPCs and that ATAD2 and BRD2 have prognostic value. Finally, we developed gene stratification

signature (BROMO-10) for bromodomain response and PC prognostication, to inform current and future trials with drugs targeting these processes. Our findings provide a compelling rational for combination therapy targeting bromodomains in selected patients in which BRD-mediated TF binding is enhanced or modified as cancer progresses.

INTRODUCTION

Prostate cancer (PC) is the most common male cancer in the United States and Europe (Center et al., 2012). Androgen receptor (AR) signaling is required for the development of the prostate gland and is maintained in PC including at the stage of progression to castration-resistant prostate cancer (CRPC) (Zhang et al., 2013).

CRPC is characterized by copy number gain at the AR locus occurring in around 30% of advanced cases. Consequently AR is overexpressed in these tumors. However, AR deregulation is also a frequent feature (>90%) of advanced castrate-resistant cases (Waltering et al., 2012), which persist after resistance to antiandrogens such as enzalutamide and abiraterone (Buttigliero et al., 2015). We have previously shown that AR deregulation is associated with local chromatin landscape changes, which are able to reinforce the binding of AR to chromatin even in low androgen environments (Urbanucci et al., 2012a, 2012b). This mimics the conditions occurring in CRPC (Xu et al., 2006). Phenotypically, AR deregulation results in increased growth rates even under conditions of androgen deprivation (Waltering et al., 2009). Moreover, genome-wide AR recruitment to chromatin is detectable in such conditions (Andreu-Vieyra et al., 2011), suggesting that the chromatin is open and in some way primed by pre-docked AR even before the cells are treated with hormones. Androgen treatment then enhances AR recruitment (Urbanucci et al., 2012a). This suggests that nucleosome positioning is predetermined in PC cells, a hypothesis that has been confirmed by a recent study (Chen et al., 2015).

Clinical epigenetics, defined as functionally relevant changes to the genome that do not involve a change in the nucleotide sequence and impact on disease phenotypes, is becoming extremely important for cancer detection and treatment. One indirect assessment of epigenetic alteration is the accessibility of DNA, determined by DNase hypersensitivity analysis or by formaldehyde-assisted isolation of regulatory elements (FAIREs) (Song et al., 2011).

Proof of a de-regulated epigenome in CRPC includes altered patterns of DNA methylation, histone modifications (Perry et al., 2010), and increased and altered AR binding to chromatin (Pomerantz et al., 2015; Sharma et al., 2013).

In addition, epigenetic readers such as bromodomain-containing protein 4 (BRD4) have been shown to associate with transcription factors (TFs) such as AR (Asangani et al., 2014; Nagarajan et al., 2014; Shi and Vakoc, 2014) and contribute to aggressive cancers of many types (Delmore et al., 2011; Shi and Vakoc, 2014) including PC (Asangani et al., 2014; Wyce et al., 2013). Nevertheless, the underlying mechanisms of action of bromodomain inhibitors have not yet been completely elucidated (Shi and Vakoc, 2014). Therefore, we set out to investigate the underlying global changes in chromatin accessibility as a driver of cancer progression (Lever and Sheer, 2010; Timp and Feinberg, 2013).

Here, we report that DNA accessibility alone is able to discriminate advanced prostate tumors from earlier disease states and benign tissue. The chromatin of these tumors is more accessible due to indirect mechanisms in which the AR plays a role. We show that BRDs, such as BRD4 and androgen-regulated BRD2 and ATAD2, are the mediators of such increased accessibility and are prognostic tissue markers overexpressed in CRPC. Finally we provide a ten-gene signature, BROMO-10, that can be used to stratify patients with poorer outcome and guide PC patient selection for combinatorial trials of bromodomain and extra-terminal (BET)-targeted therapies with other agents.

RESULTS

Deregulation of the AR Enhances Bromodomain-Mediated Chromatin Opening in Advanced Tumors

To understand whether progression to CRPC is associated with global changes in chromatin accessibility, we assessed chromatin opening and DNA regions with regulatory activity in three benign prostate hyperplasia (BPH), three primary untreated PC, and three locally recurrent CRPC samples using FAIRE sequencing (FAIRE-seq) (Giresi and Lieb, 2009).

One-third of the genome consisted of open regions of chromatin in two CRPC samples, whereas only about one-sixth of the genome comprised open chromatin in the other samples (Figure 1A and Table S1A). We validated open chromatin regions via FAIRE-qPCR at prostate specific antigen (PSA) and TMPRSS2 gene loci, showing enhanced chromatin opening in CRPC (Figure 1B).

We built disease-stage-specific high-confidence consensus open chromatin maps. On average, only 15% of the FAIRE-seq sites overlapped between the samples (Table S1A) highlighting epigenetic heterogeneity. We found that the majority of open sites were unique to CRPC samples (Figure 1C) and were larger than in PC or BPH (Figure S1A). To classify disease stage, we used principal component analysis of the FAIRE-seq data and found that in terms of chromatin state, CRPC chromatin appeared more diverse when compared with BPH or PC (Figure 1D), indicating that extensive chromatin remodeling is a late event in PC progression.

RNA sequencing (RNA-seq) of the same clinical samples showed a positive correlation between upregulated genes and an open chromatin state (Figure 1E) up to 250 kb upstream the transcriptional start sites (TSSs) (Figure 1F). In agreement with published studies (Cedar and Bergman, 2012), DNA methylation profiles obtained for the same clinical samples showed a negative correlation with gene expression within 1 and 5 kb around the genes' TSS (Figure 1G). Importantly, such correlations were independent of sample type, indicating conserved mechanisms across all disease stages.

Next, to investigate the effect of the AR deregulation on chromatin opening, we performed FAIRE-seq in CRPC cells such as lymph node carcinoma of the prostrate (LNCaP) and

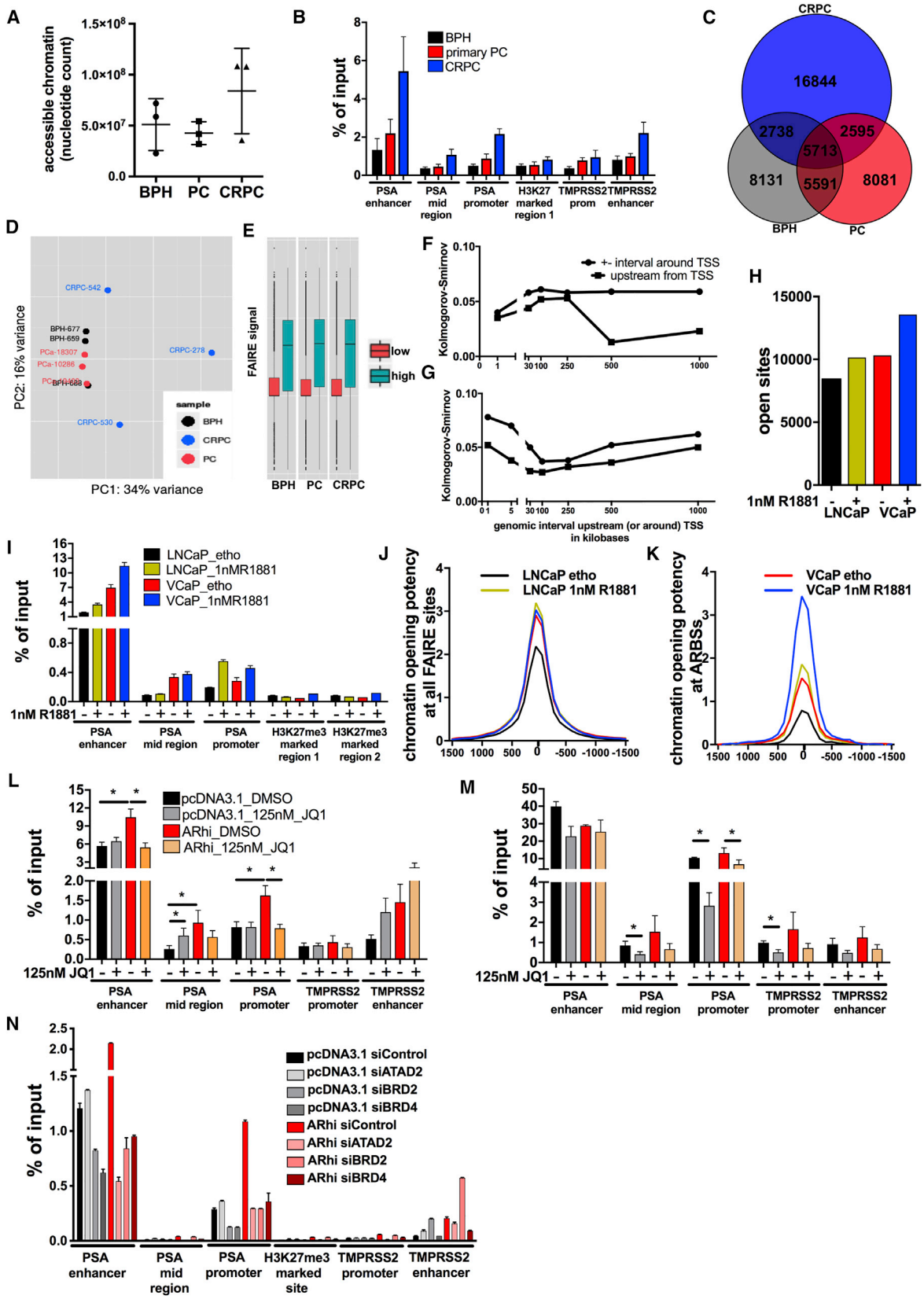

(legend on next page)

vertebral-cancer of the prostate (VCaP) cultured in the presence and absence of androgens. VCaP cells overexpress the AR compared to LNCaP due to AR gene locus amplification (Urbanucci et al., 2013). More FAIRE-seq sites were found in VCaP than in LNCaP cells (Figure 1H and Table S1A), and VCaP cells also showed a greater increase in the number of FAIRE-seq sites in the presence of androgens (Figure 1H).

One-third of the FAIRE-seq sites were present in both cell lines (Figure 2A). Androgen treatment reprogrammed chromatin accessibility affecting 20%–50% of sites (Figure 2B).

80% of common FAIRE-seq sites were conserved between cell lines and tissue samples (Table S1B). Chromatin opening measured via FAIRE-qPCR at PSA (Figure 1I) and TMPRSS2 (Figure 2C) loci or measured in silico genome-wide (Figures 1J and 2D–2F) was greater in VCaP cells than in LNCaP cells. An average of 21% of clinically relevant AR binding sites (ARBSs) in CRPC tissue (Sharma et al., 2013) and 45% E26 transformation-specific or E-twenty-six family (ETS)-related gene (ERG) binding sites (ERGBSs) in VCaP cells (from Yu et al., 2010) overlapped with FAIRE sites (Table S1B).

Androgens enhanced chromatin opening at FAIRE sites overlapping with CRPCs' ARBSs and ERGBSs only in LNCaP cells (Figures 2D and 2E), while they had no effect in VCaP cells. In VCaP cells, androgens enhanced chromatin opening at matched cell lines ARBSs (Figure 1K) and at ARBSs present in cell lines and tumors (Figure 2F) but not at ERGBSs (Figure 2E).

To validate the role of AR in chromatin opening, we used an LNCaP-based model expressing endogenous and increased AR levels (Waltering et al., 2009) (Figure 2G) and confirmed enhanced chromatin opening in AR-overexpressing cells at the PSA and TMPRSS2 loci. These data suggest that both AR deregulation and androgens affect chromatin opening in CRPC cells at ARBSs, but not at ERGBSs.

Distribution of FAIRE-seq sites in clinical samples and cell lines showed increased opening at intronic/intergenic regions (Figures S1B–S1I), which is in agreement with previous findings showing increased AR chromatin binding at these regions (Sharma et al., 2013; Urbanucci et al., 2012b).

Given that chromatin remodeling is not exclusively associated with ARBSs, we tested whether enhanced chromatin opening was associated with the presence of different motifs in CRPC by performing motif analysis on FAIRE site maps of tissue samples and cell lines (Table S1C). Consistent with its role in maintaining chromatin compaction (Tark-Dame et al., 2014), CCCTC-binding factor (CTCF)-like motifs were among the top enriched motifs in both clinical specimens and cell lines, followed by ETS-like motifs. CTCF and ETS motifs were enriched in all clinical specimens, including common sites, while c-MYC motifs were exclusively present in open regions found in CRPC samples. Nuclear transcription factor Y subunit (NFY) and SP1 motifs were highly enriched in both treatment conditions in both cell lines. Although they were not enriched at FAIRE sites in tumors, NFY and SP1 have been shown to be involved in chromatin regulation and to have a potential role in cancer progression (Dolfini and Mantovani, 2013; Tewari et al., 2012). Interestingly, forkhead box (FOX)-like motifs were significantly enriched only in the LNCaP FAIRE sites (Table S1C). This suggests that only a subset of FAIRE sites, those that may overlap with ARBSs, are regulated by FOXA1, and other chromatin remodelers may play a role.

Therefore, we sought to understand whether enhanced chromatin opening in the context of AR deregulation favors chromatin binding of different proteins such as nuclear transcription factor Y subunit alpha (NFYA), the regulatory subunit of the NFY complex (Dolfini and Mantovani, 2013), and c-Myc.

We retrieved publicly available consensus binding data from ENCODE. Overlap of FAIRE-seq data with ENCODE data on chromatin binding of CTCF, MYC, and NFYA showed that, on average, 44% of the ENCODE NFYA sites, 18% of MYC sites, and only 12% of CTCF sites lay within the open chromatin sites (Table S1D). However, no significant increase or decrease of overlapping sites was observed in CRPCs, which may be due

Figure 1. Deregulation of AR Favors Bromodomain-Mediated Chromatin Opening in Castration-Resistant Prostate Cancer

(A) Number of nucleotides located within open chromatin peaks identified via formaldehyde-assisted isolation of regulatory elements followed by sequencing (FAIRE-seq) in three benign prostate hyperplasia (BPH), three primary prostate cancer (PC), and three locally recurrent castration-resistant prostate cancer (CRPC) tissue specimens.

(B) FAIRE-qPCR validation of local chromatin opening at the PSA and TMPRSS2 loci in the clinical samples. An H3K27me3 marked region was used as negative control (closed region).

(C) Overlap of open chromatin regions commonly found in BPH, PC, or CRPC samples according to the FAIRE-seq analysis.

(D) Principal component analysis of three benign and six cancer (three primary and three CRPC) prostate tissue samples according to chromatin shape.

(E) Association between local chromatin opening, up to 1 kb upstream the genes transcription start site, and gene expression in matched tissue samples, according to RNA-seq.

(F and G) Analysis of Kolmogorov-Smirnov statistical test values describing the deviation of correlative events between matched gene expression and local chromatin accessibility (F) or local DNA methylation (G) from a random set of associative events of the same type, in all nine clinical samples. Local chromatin accessibility and DNA methylation were measured at the indicated intervals and correlated in a gene-wise manner to respective gene expression in the same tissue (see Figure S4 for details).

(H) Number of open chromatin regions found by FAIRE-seq analysis of LNCaP and VCaP cells treated with 1 nM R1881 or vehicle.

(I) FAIRE-qPCR validation of local chromatin opening at the PSA locus in LNCaP and VCaP cells treated with 1 nM R1881 or vehicle.

(J and K) Chromatin opening potency assessed by FAIRE-seq reads distribution around all FAIRE-seq sites (J) or around matched androgen receptor binding sites (ARBSs) (K) in LNCaP and VCaP cells treated as above.

(L–N) FAIRE-qPCR analysis of local chromatin opening at the PSA and TMPRSS2 loci in a LNCaP-based AR overexpression model (*$p < 0.05$ according to t test). FAIRE-qPCR in LNCaP-pcDNA3.1 and -ARhi cells following 4 days of hormone starvation (L) or without starvation (full serum) (M), treated with 125 nM JQ1 (+) or vehicle (DMSO) (–) (*$p < 0.05$ according to t test). (N) FAIRE-qPCR upon transfection with siRNA control or siRNA against ATAD2 (siATAD2), BRD2 (siBRD2), or BRD4 (siBRD4) (two biological repeats with three technical replicates each).

Error bars represent SEM. See also Figure S1 and Tables S1A–S1D.

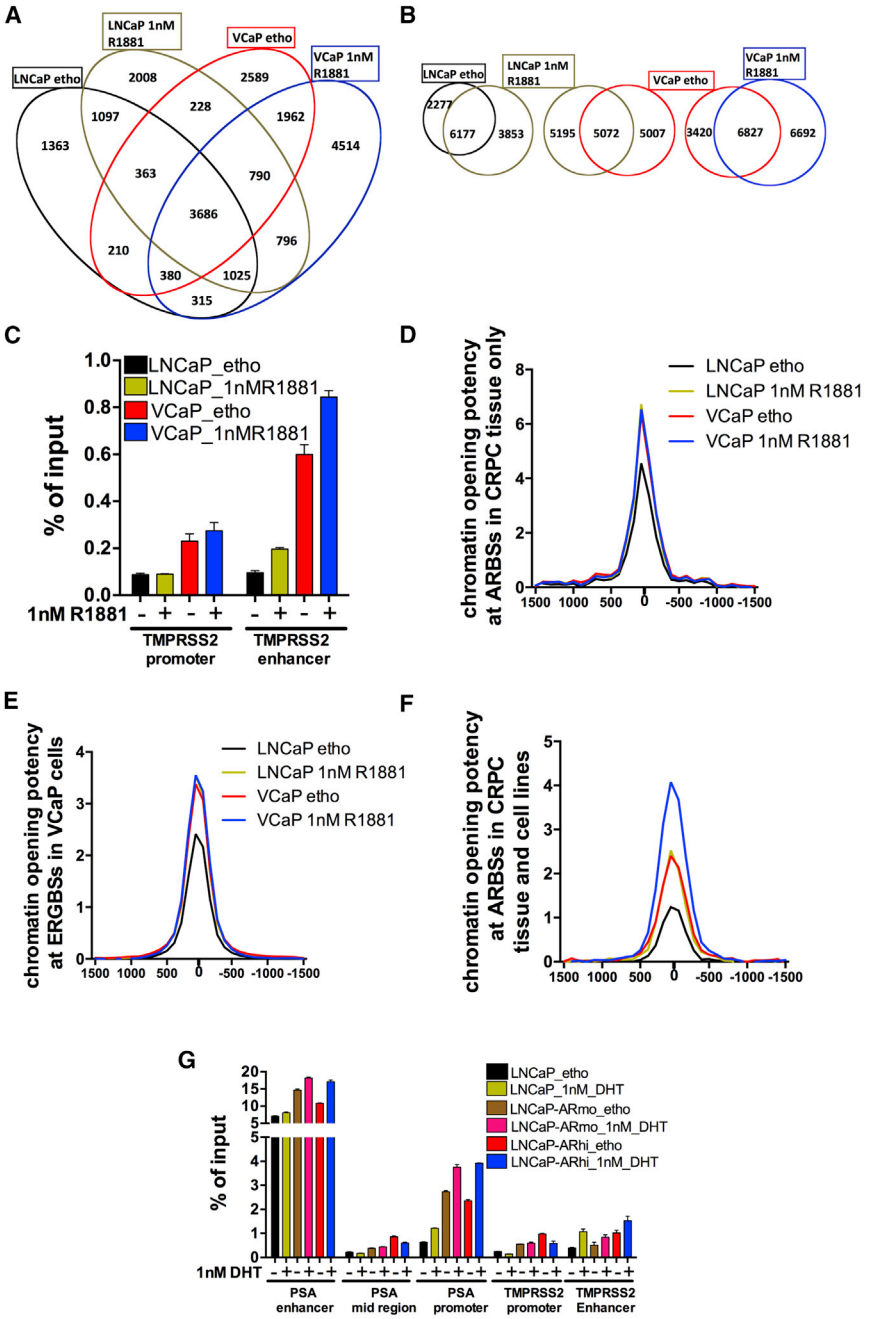

Figure 2. AR Overexpression in Castration-Resistant PC Cell Models Is Associated with Increased Open Chromatin

(A and B) Multi-parametric comparison showing open chromatin regions found by FAIRE-seq analysis in LNCaP and VCaP cells treated with 1 nM R1881 or vehicle (etho, ethanol) (A). Three pairwise comparisons of open chromatin regions—LNCaP treated with R1881 or ethanol; LNCaP treated with R1881 versus VCaP treated with ethanol and VCaP treated with R1881 or ethanol (B).

(C) FAIRE-qPCR validation of local chromatin opening at the TMPRSS2 locus (Urbanucci et al., 2012a) in two cell lines with and without hormone or vehicle.

(D–F) Chromatin opening around (D) androgen receptor binding sites (ARBS) in CRPC (Sharma et al., 2013), (E) ERG binding sites (ERGBS) (Yu et al., 2010), and (F) ARBS conserved between CRPC tissue and cell lines (Sharma et al., 2013).

(G) FAIRE-qPCR validation of chromatin opening at PSA and TMPRSS2 loci (Urbanucci et al., 2012a) in a LNCaP-based AR overexpression model (Waltering et al., 2009) treated with hormone or vehicle.

Error bars represent SEM.

to cell specificity of the TF binding or due to tissue heterogeneity (data not shown).

BRDs are druggable chromatin readers that recognize acetylated histones (Filippakopoulos et al., 2012) and modulate transcription in cancer-associated genes (Filippakopoulos and Knapp, 2014; Lovén et al., 2013). Since we showed that histone acetylation is increased in AR-overexpressing cells (Urbanucci et al., 2012a), we hypothesized that BRDs would mediate chromatin opening. To test our hypothesis, we used the pan-BET bromodomain inhibitor JQ1 to assess the impact on chromatin opening potency at selected loci.

In hormone-starved cells, JQ1 treatment induced chromatin closure in AR-overexpressing cells, but had little or no effect in parental cells (Figure 1L). In the presence of androgens, JQ1 had a stronger effect on parental than on AR-overexpressing cells (Figure 1M), highlighting the role of androgens in chromatin opening. In addition to BRD2/4 as the main targets of JQ1, we also evaluated ATAD2, since it has been reported that this BRD is a common coactivator of AR and MYC.

RNAi knockdown of the BET proteins BRD2 and BRD4 reduced PSA enhancer and promoter opening in AR-overexpressing cells, but in parental cells ATAD2 knockdown did not (Figure 1N). Interestingly, at the TMPRSS2 enhancer only BRD4 knockdown was effective in reducing chromatin opening, suggesting that compensatory events occur if a specific BRD is targeted.

Based on these data, we hypothesized that the expression of some BRDs might be AR dependent. To test androgen regulation of BRDs genes we validated proximal ARBSs (Data S1) identified in publicly available datasets. Chromatin immunoprecipitation at ATAD2 and BRD2 proximal ARBSs showed stronger AR binding than BRD4 proximal ARBS. The strongest ARBS to BRD4 was located 200 kb from the TSS (Figure 3A). ATAD2 and BRD2 transcripts were induced by androgen (the latter only modestly), while BRD4 transcript was not (Figure 3B). AR

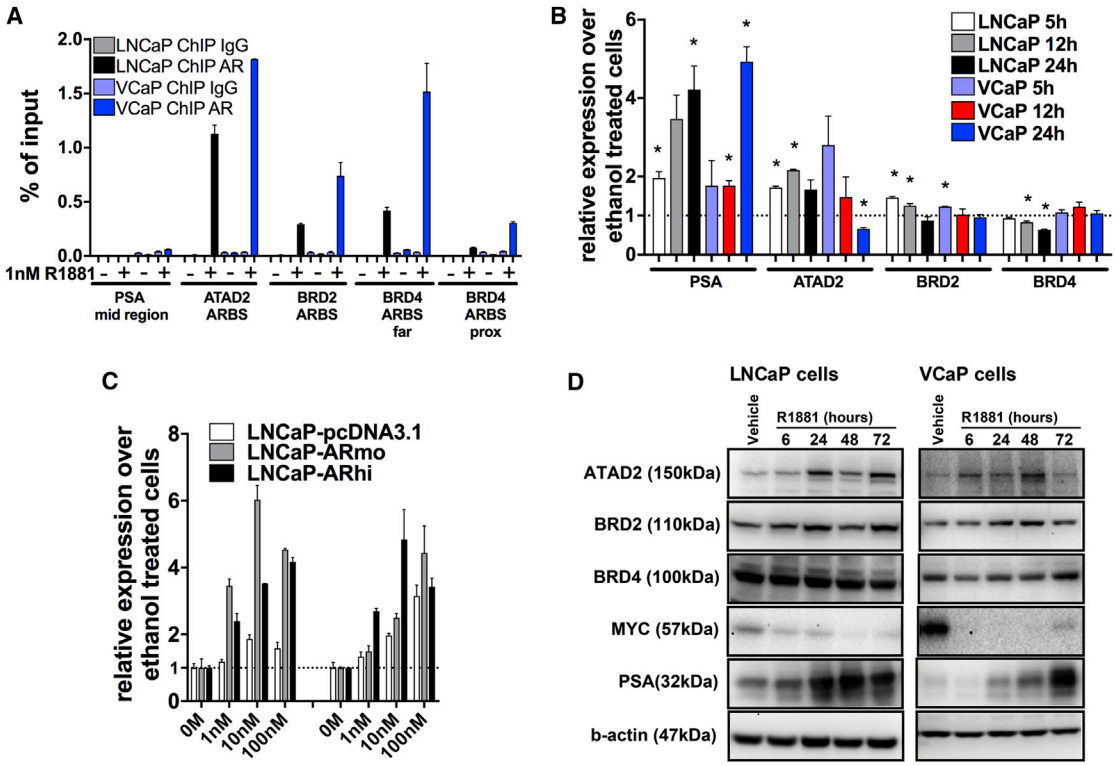

Figure 3. Androgens and AR Regulate BRDs Expression

(A) Androgen receptor binding sites (ARBSs) close to BRD4, BRD2, and ATAD2 genes according to publicly available datasets (see Data S1) were validated by chromatin immunoprecipitation (ChIP)-qPCR analysis. PSA mid-region served as ARBS negative control.

(B) Indicated transcript levels measured by qRT-PCR after hormone treatment.

(C) ATAD2 gene expression measured by qRT-PCR in LNCaP-pcDNA3.1, -ARmo, and -ARhi treated with hormone. The mean and SEM of ATAD2 against TATA-binding protein (TBP) values normalized measure with no treatment (0M).

(D) Western blot analysis of indicated proteins levels in cells treated with hormone.

See Figure S2.

overexpression sensitized ATAD2 transcription to lower concentrations of androgens (Figure 3C). In contrast to BRD4, ATAD2 and BRD2 protein levels were increased in AR-overexpressing cells and further increased by androgen stimulation (Figures 3D and S2A). AR knockdown in LNCaP cells during a time course of androgen treatment reduced ATAD2 transcript and protein levels within 24 hr (Figures S2B and S2C). In contrast, BRD2 protein levels were downregulated only after 48 hr treatment with AR-targeted small interfering RNA (siRNA) (Figure S2C).

BRDs Are Tissue Biomarkers Overexpressed in Castration-Resistant PCs

To establish the predictive clinical value of BRD2/4 and ATAD2, we performed qRT-PCR (Figures 4A–4D) and immunohistochemical (IHC) analyses (Figures 4E–4H) using benign prostate tissue and PC specimens and found that all transcripts were overexpressed in cancer compared to BPH. The long form of BRD4 (BRD4-L) ($p > 0.05$) and BRD2 ($p < 0.0001$) nuclear staining was increased in CRPC (Figures 4I and 4J). BRD4 (Figure S3A) and BRD2 (Figure 4K) protein levels determined by IHC were not prognostic for biochemical recurrence, although BRD2 staining separated patients with poor prognosis and was significantly ($p = 0.0154$) associated with mortality (Figure 4L). Strong nuclear (Figure 4M) and cytoplasmic (Figure S3B) staining for ATAD2 was significantly increased in CRPC cases ($p < 0.0001$). Moreover, strong nuclear (Figure 4N) but not cytoplasmic (Figure S3C) staining was associated with poor outcome (Figure S3D). We confirmed the significant ($p < 0.001$) prognostic relevance of ATAD2 as a tissue biomarker for biochemical recurrence in an independent cohort of 12,427 patients' samples (Figures 4O and S3). Positive staining for ATAD2 was associated with Ki67 staining, tumor stage, and AR protein expression (Figure S3).

Androgen-Receptor-Overexpressing Cells Are More Sensitive to Bromodomain Inhibitors

BRD inhibitors have been reported to reduce the viability of PC cells (Asangani et al., 2014). To determine whether these effects are dependent on AR expression levels, we performed knockdowns of BRDs in AR-overexpression cell models in the presence of androgens (Figures S4A and S4B). Silencing BRD4 decreased MYC levels in both LNCaP and VCaP cells, while upregulating slightly AR, and PSA only in VCaP cells (Figure S4B). Knockdown of BRD4 decreased viability in all the AR-positive cell lines tested (LNCaP-pcDNA3.1, LNCaP-ARhi, and VCaP),

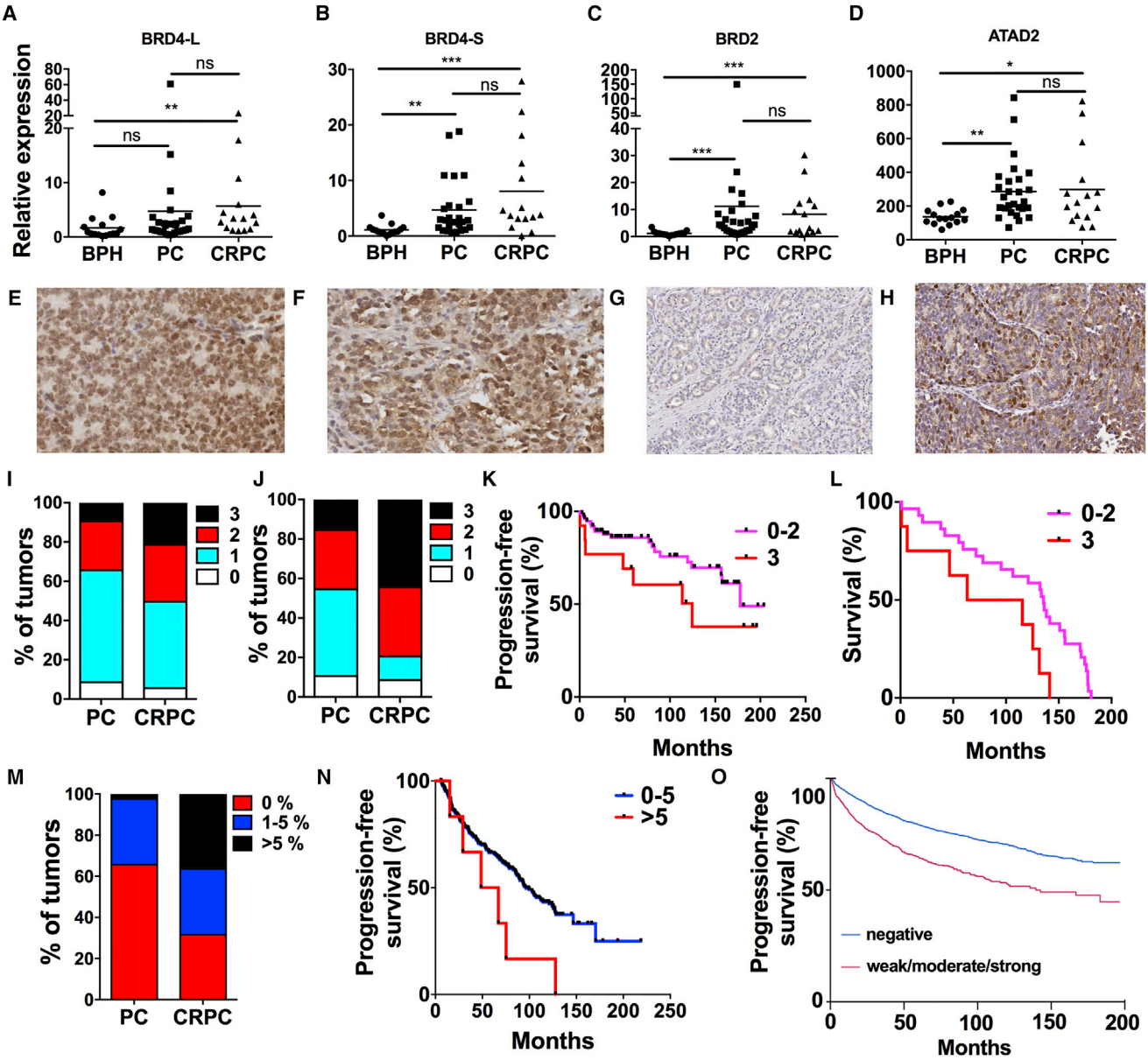

Figure 4. BRDs Are Tissue Biomarkers Overexpressed in Castration-Resistant PC

(A–D) Expression of BRD4-long (BRD4-L) (A), BRD4-short (BRD4-S) transcript form (B), BRD2 (C), and ATAD2 (D) gene transcripts relative to TBP levels in BPH (n = 15), primary untreated PC (n = 27), and CRPC (n = 15) specimens according to qRT-PCR. Kruskal-Wallis with Dunn post-test results are shown (***p < 0.0001; **p < 0.001; *p = 0.01–0.05; ns, not significant).

(E and F) CRPC immunohistochemical (IHC) strong stainings (score = 3) for BRD4 long isoform (E) and BRD2 (F).

(G and H) CRPC IHC stainings showing examples of low (0%) (G) and high (<5%) (H) staining of nuclear ATAD2. Images are 8× magnification.

(I and J) Proportions of tumors according to BRD4 long isoform (I) and BRD2 (J) staining intensity in PC (n = 159 for BRD4 and n = 90 for BRD2) and CRPC (n = 128 for BRD4 long isoform and n = 34 for BRD2).

(K) Kaplan-Meier analysis of biochemical progression-free survival in 90 prostatectomy-treated patients according to BRD2 stainings (p = ns calculated with Mantel-Cox test).

(L) Kaplan-Meier analysis showing shorter time to death in 37 men that died of PC out of the 90 patients for which material was stained for BRD2 (p = 0.015 calculated with Mantel-Cox test).

(M) Proportions of tumors according to percentage of ATAD2 positive nuclei in PC (n = 258) and CRPC (n = 121) specimens (p < 0.0001 according to X^2 test).

(N) Kaplan-Meier analysis of biochemical progression-free survival in prostatectomy-treated patients according to the percentage of ATAD2 positive nuclei. Six patients with high frequency of ATAD2-positive nuclei had very short progression-free time (p = 0.0354 calculated with Mantel-Cox test).

(O) Kaplan-Meier analysis of biochemical progression-free survival in a validation cohort of 8,541 prostatectomy-treated patients according to ATAD2 staining (p < 0.001). 26% (n = 2,216) of the stainings were positive for ATAD2, of which strong ATAD2 staining accounted for 81% (n = 1,789).

Error bars represent SEM. See Figure S3.

but knockdown of BRD2 or ATAD2 alone had no effect on viability (Figure 5A). ATAD2 inhibition via a small molecular probe was shown to have limited effect on viability of LNCaP cells (Bamborough et al., 2016). Silencing ATAD2 upregulated AR specifically in LNCaP and MYC in VCaP cells, while silencing BRD2 slightly upregulated MYC in both LNCaP and VCaP cells (Figure S4B). Therefore, our data suggest that compensatory mechanisms such as enhanced AR/MYC signaling may take place and promote cell survival when single BRDs are targeted. In fact, co-targeting both ATAD2 and BRD2 in LNCaP cells via a combinatorial knockdown had no additive effect on decreasing cell viability compared to targeting BRD2 alone (Figure 5B) and highlighted that BRD4 is important but not the only contributor to cell viability.

To test whether AR deregulation enhances sensitivity to bromodomain inhibitors, we treated a panel of AR-positive PC cell lines with JQ1 in the presence of androgens (Figures 5C, S4C, and S4D). AR levels in 22RV1 and LNCaP cells are similar (Erzurumlu and Ballar, 2017), while LNCaP-ARhi and VCaP cells overexpress AR compared to LNCaP (or LNCaP-pcDNA3.1) with VCaP showing the highest levels of AR (Urbanucci et al., 2012b; Waltering et al., 2009). VCaP cells were indeed the most sensitive cells to JQ1 treatment. LNCaP-ARhi and parental LNCaP cells were equally responsive to JQ1 treatment (Figure S4D). However, when such cells were grown in androgen deprivation conditions (castrate conditions), AR-overexpressing cells were more sensitive to JQ1 (Figure 5D). Also, combined treatment with enzalutamide and JQ1 was more effective in AR-overexpressing cells (Figures 5E and 5F), suggesting that AR deregulation is implicated in response to BET inhibition.

Combined treatment with JQ1 and enzalutamide triggered apoptosis in VCaP cells in full media (Figure 5G), but not in LNCaP cells, even when deprived of androgens (Figures S4E and S4F). This indicates that AR activity/level defines whether this drug combination has a cytostatic (low-level AR activation) or cytotoxic (high-level AR activation) effect.

When cells are treated with anti-androgens, resistance can emerge in which AR activity is maintained (Buttigliero et al., 2015). Using an enzalutamide-resistant LNCaP model (Kregel et al., 2013), we found that the inhibitory effect of JQ1 was retained (Figure 5H).

Gene Expression Analysis of Bromodomain Inhibitor-Treated Cells and Six Independent PC Cohorts Reveal a Ten-Gene Signature for Patient Stratification

To identify patients that could potentially benefit from BET-targeted therapies, we sought to identify a gene signature able to stratify CRPC responders. We performed a time-course treatment with JQ1 in LNCaP (Figure S5A) and VCaP (Figure S5B) cells to identify affected genes. Upregulated genes (Table S2A) showed significant overrepresentation of histone genes (Figures S5C and S5D) and overrepresentation of GO terms for chromatin compaction ($p < 10^{-6}$) (Table S3), corroborating the tendency for chromatin closure upon JQ1 treatment, while downregulated transcripts (Table S2B) included AR targets found in tissues of CRPC patients (Sharma et al., 2013) (Figure 6A). We validated decreased protein levels of the AR targets PSA and CAMKK2 upon JQ1 treatment (Figure S2A). CRPC-associated genes such as UBE2C, HOXB13, AURKA, and CAMKK2 (Data S1) that were downregulated by JQ1 treatment (Figures S5E and S5F) and affected by BRD4 knockdown (Figure S5G) also showed bromodomain-dependent local chromatin opening (Figure S5H). AR deregulation affected chromatin opening especially at ARBSs, when present (Figures S5I and S5J).

Finally, we used published clinical expression array data (Taylor et al., 2010) and RNA-seq of clinical specimens (Ylipää et al., 2015) to identify a clinical gene signature of overexpressed genes in CRPC (Tables S4A and S4B). We compared lists of CRPC-overexpressed genes with those that displayed increased proximal chromatin opening in CRPC (Figure 6B and Table S5) and genes downregulated by JQ1 treatment in cell lines and obtained a set of 15 genes (Figures 6C and 6D).

A generalized linear model with elastic net regularization (Erho et al., 2013) was used on the Mayo Clinic I (MCI) PC cohort (Erho et al., 2013) as the discovery dataset to assess the association of the 15 genes to biochemical recurrence, PC specific mortality, and metastatic recurrence. Ten of the 15 genes contributed significantly to the model.

We called the resulting ten-gene signature "BROMO-10." To evaluate the prognostic significance of BROMO-10, first we used RNA-seq data from an independent cohort of PC from the Fred Hutchinson Cancer Research Center (Kumar et al., 2016; Roudier et al., 2016) (Figures 6E and 6F). Genes comprising the signature were deregulated in this cohort with seven out of ten genes being differentially expressed when comparing CRPCs to primary PCs.

Next, we assessed the independent prognostic value of each gene according to various endpoints in two additional validation cohorts (Karnes et al., 2013; Ross et al., 2016) (Table S6).

According to univariable and multivariable analysis, BROMO-10 contributed independent prognostic information over the clinicopathological variables. In the Johns Hopkins Medical Institutions-Radical Prostatectomy (JHMI-RP) cohort of high-risk men treated with radical prostatectomy without adjuvant or salvage therapy prior to metastatic onset, BROMO-10 discriminated for the biochemical recurrence endpoint (Figures 7A, S6A, and S6B) and the PC-specific mortality endpoint in the MCII cohort of high-risk men (Figures 7B, S6C, and S6D).

We further assessed the prognostic value of BROMO-10 in predicting the onset of CRPC. Fifty-five patients that developed metastasis after radical prostatectomy without any adjuvant or salvage therapy ("natural history cohort") treated at Johns Hopkins were evaluated using Kaplan-Meier analysis considering time to CRPC from metastatic onset. Upon metastatic onset, all patients received androgen deprivation therapy (ADT). Higher BROMO-10 scores were associated with an increased rate of CRPC after ADT (Figure 7C). The upper quartile of BROMO-10 signature scores had a median time to CRPC of 12 months compared to the lower quartile of 84 months ($p = 0.01$).

Finally, to assess whether BROMO-10 is able to predict responsiveness of PC to bromodomain inhibitors, we used RNA-seq profiles of panels of PC cell lines and expression array profiles of patient-derived xenografts (PDXs) (Nguyen et al., 2017) to generate BROMO-10 scores (Figures 7D and 7E). We then correlated these scores with publicly available IC_{50} data for JQ1 (Asangani et al., 2016) (Figure 7F), ZEN-3694 (Attwell

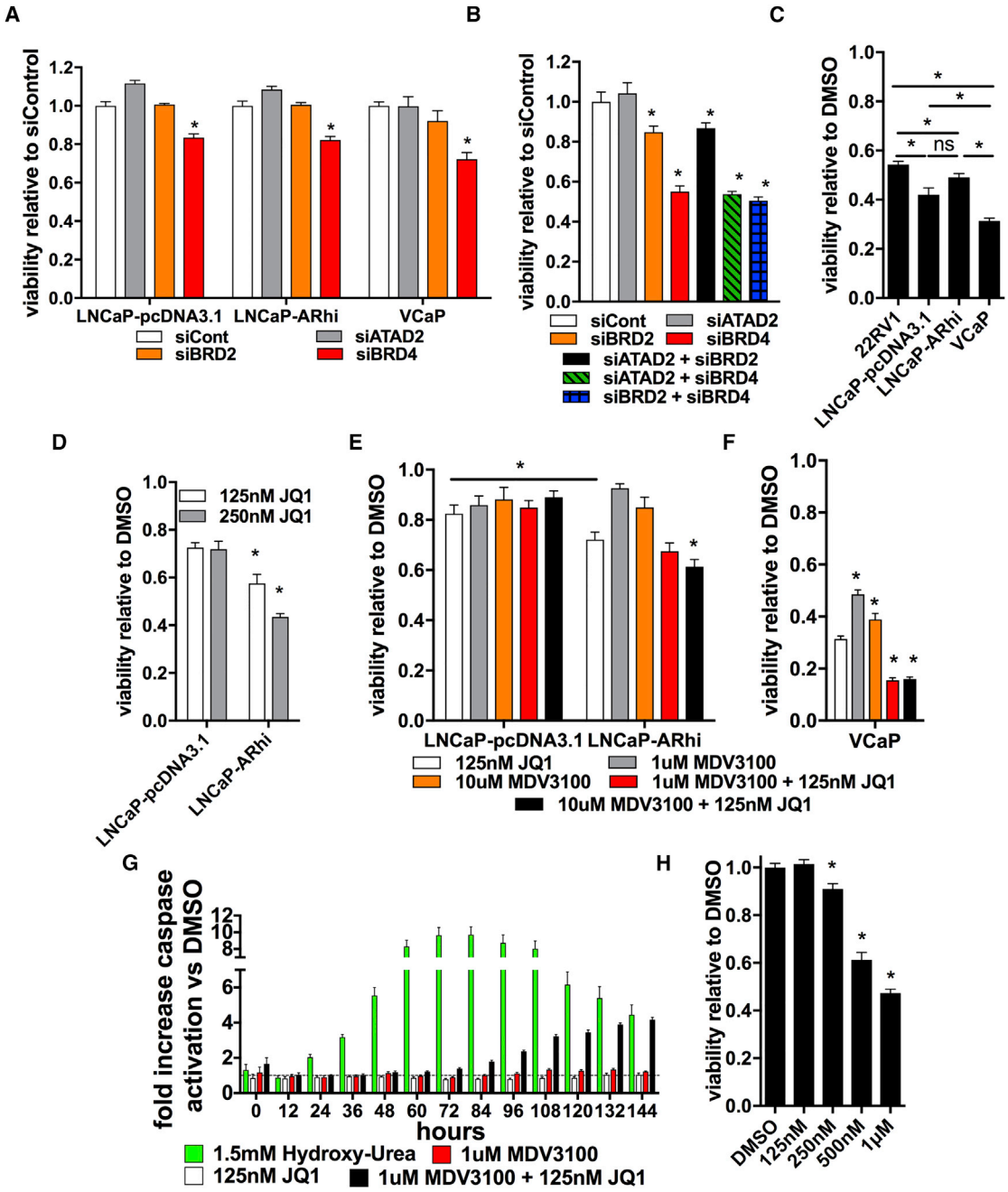

Figure 5. Impact of Bromodomain Inhibition on PC Cell Viability Is Enhanced by AR Deregulation

(A) Viability of LNCaP-pcDNA3.1, LNCaP-ARhi, and VCaP cells 3 days after transfection with siControl (siCont), siBRD2, siATAD2, or siBRD4, relative to control siRNA values.

(B) Viability of parental LNCaP cells 3 days after transfection with siRNA as indicated. *$p < 0.05$ according to t test versus the siCont column. n = 6 for each replicate, for each condition. Each experiment was repeated three times.

(C) Relative viability of 22RV1, LNCaP-pcDNA3.1, LNCaP-ARhi, and VCaP cells cultured in full serum and treated with DMSO or JQ1(*$p < 0.05$ according to t test between the indicated conditions).

(D) LNCaP-pcDNA3.1 and -ARhi cells were treated with 1 nM DHT as well as JQ1 or vehicle (DMSO).

(E and F) Solo or combinatorial treatment of LNCaP-pcDNA3.1 and LNCaP-ARhi cells (E) or VCaP cells (F) with MDV3100 and JQ1. Viability compared to DMSO was assessed after 3 days treatment (*$p < 0.05$ according to t test versus JQ1 treatment alone).

(G) Caspase activation assay upon treatment of VCaP cells with JQ1, MDV3100, or a combination; hydroxyl-urea was used as a positive control.

(H) Viability of MDV3100-resistant LNCaP cells treated with JQ1(*$p < 0.05$ according to t test versus DMSO).

Refer also to Figure S4.

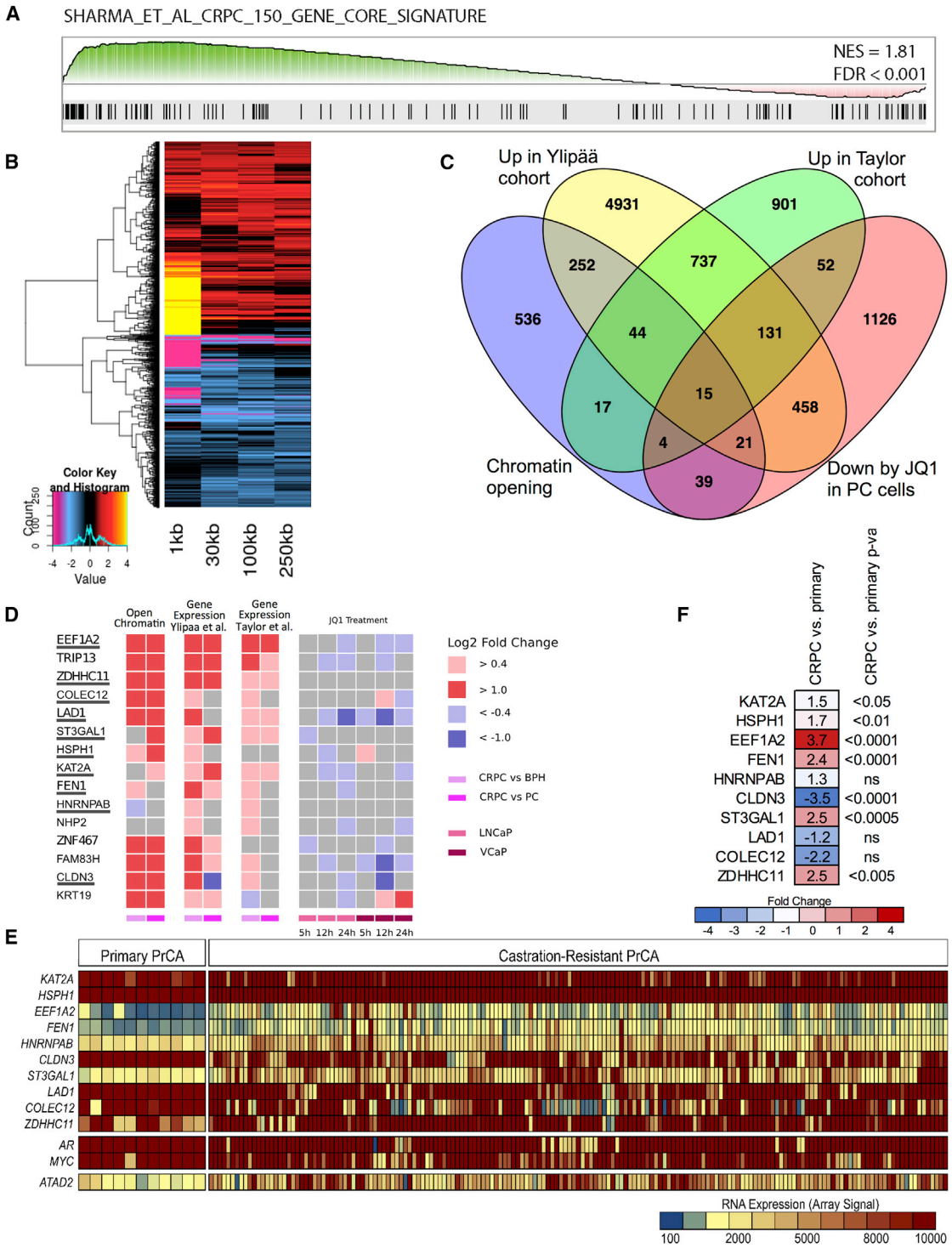

Figure 6. Bromodomain Inhibition Targets Clinically Relevant Transcriptional Program Useful for Selecting Patients Responsive to Bromodomain-Targeted Therapies

(A) GSEA of AR target gene signature (150 core genes identified in CRPC tissue) (Sharma et al., 2013) in expression analysis of VCaP cells treated with JQ1.

(B) Heatmap of genes displaying differential chromatin opening (varying distances upstream of TSSs) in CRPC versus primary PC.

(C) Overlaps between overexpressed genes in CRPC in two clinical microarray datasets (Tables S4A and S4B), the genes associated with open chromatin sites in CRPC (Table S5) and the consensus genes downregulated by JQ1 treatment of two cell lines (Table S2B).

(D) 15 genes associated with open chromatin, overexpressed in CRPC and downregulated by JQ1 treatment.

(legend continued on next page)

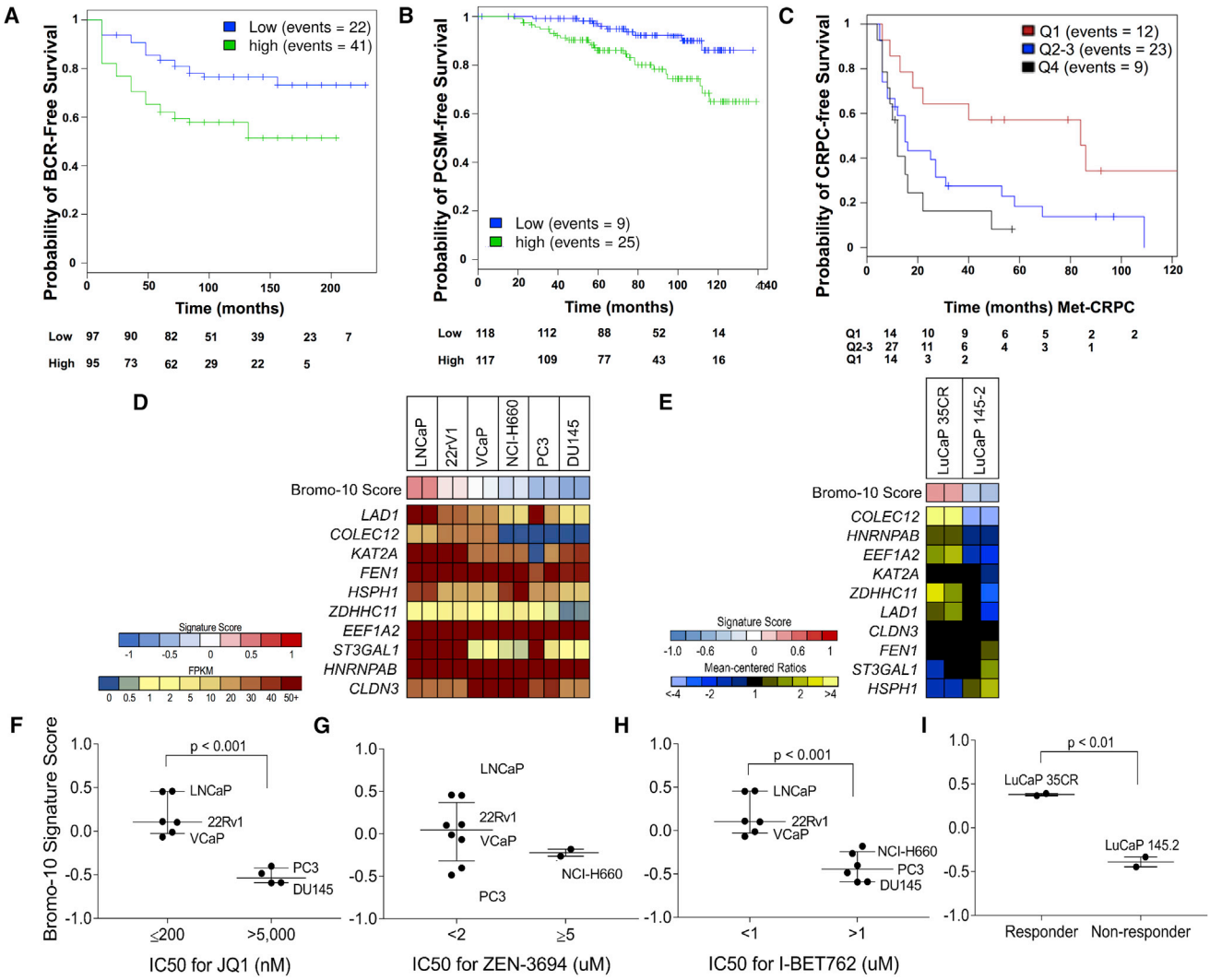

Figure 7. Prognostic and Predictive Value of the Ten Genes Signature BROMO-10

(A–C) Kaplan-Meier curves indicating the prognostic separation achieved by high and low BROMO-10 scores versus (A) biochemical recurrence in the JHMI-RP validation cohort (Ross et al., 2016) (p = 0.008) (B) prostate cancer-specific mortality (PCSM)-free survival in the Mayo Clinic validation cohort (Karnes et al., 2013) (p = 0.0089) and (C) CRPC-free survival of patients post-ADT treatment of metastatic patients in the JHMI cohort as expression quartiles (n = 55, p value 0.01).
(D and E) Heatmaps of BROMO-10 score and individual gene expression in cell lines (D) and also in PDX models (E).
(F–I) Two-sample t test evaluation of the significance of growth inhibition or reduction in tumor volume with IC_{50} dose administration of BET bromodomain inhibitors JQ1 (F), ZEN-3694 (G), and I-BET762 (H) to cell lines or of ZEN-3694 to PDX xenografts (I).
See Figure S6 and Table S6.

et al., 2016) (Figure 7G), I-BET762 (Figure 7H), and responsiveness to I-BET762 treatment measured as a significant reduction in tumor volume (Wyce et al., 2013) (Figure 7I). A high BROMO-10 score was significantly ($p < 0.001$) associated with responsiveness of PC cell lines to JQ1 and I-BET762 and reduction of tumor volume upon treatment of PC PDX models with I-BET762 ($p < 0.01$). However, the comparison between groups was not significant for responsiveness to ZEN-364 because PC3 cells, notably an AR negative PC cell line, had a low BROMO-10 score and was nevertheless sensitive to ZEN-364. Taken together, these data confirm the ability of BROMO-10 to predict responsiveness to BET inhibitors.

(E and F) Underlined genes were also significant as assessed in Fred Hutchinson Cancer Research Center (FHCRC) cohort comprising primary prostate cancers (PrCa; Roudier et al., 2016) and castration-resistant PrCa (Kumar et al., 2016) (E) with indicated fold-change values and p values according to a two-sample t test (F).
Refer also to Figure S5 and Tables S2, S3, S4, and S5.

DISCUSSION

Here, we show that chromatin accessibility increases during PC cancer progression due to mechanisms that involve the AR overexpression and the activity of BRDs. Importantly, we found that the chromatin structure in CRPC is able to classify disease stage demonstrating that genome-wide chromatin structure is reprogrammed as disease progresses, and it shows distinct features compared to primary tumors or benign tissue. Increased chromatin accessibility in PC was inferred in a recent study, although the low number of peaks found in the healthy tissue dominated the results (Stelloo et al., 2015). For the present study, we developed an advanced analysis pipeline to exclude possible confounding factors such as variations in ploidy from sample to sample (see Supplemental Information). This was essential for improved analyses because copy number variation has previously been shown to be strongly associated with poor prognosis in advance disease (Taylor et al., 2010).

Interestingly, androgens were able to enhance chromatin opening especially at ARBSs. This suggests a positive feedback loop in which the AR is able to bind more tightly to the genome due to increased opening at ARBSs. These data are concordant with our previous results showing stronger AR binding to chromatin in AR-overexpressing cells (Massie et al., 2011; Urbanucci et al., 2012b) and to other reports showing that chromatin accessibility is pre-docked prior AR binding at ARBSs (Andreu-Vieyra et al., 2011; He et al., 2010).

BRDs have gained extensive attention due to their tissue-specific capacity to modulate key transcriptional events during cancer progression (Fu et al., 2015) also in CRPC where they are therapeutically relevant (Asangani et al., 2014). We found that selected key BRDs such as ATAD2, BRD2, and BRD4 have a locus-specific effect on chromatin opening, suggesting that compensatory mechanisms may take place if BRDs are inhibited with single agents. For instance, we show that upregulation of the AR or MYC proteins occurs while inhibiting ATAD2 or BRD2 and possibly explains the limited effect of their inhibition on cell viability.

We also show that ATAD2 and BRD2 are androgen regulated. ATAD2 was previously reported to be androgen regulated (Zou et al., 2009). However, here we report that ATAD2 expression is enhanced in AR-overexpressing cells at low concentrations of androgens, and BRD4 long isoform, BRD2, and ATAD2 are all overexpressed in CRPC tissues. These results support the presence of an AR deregulation-mediated positive feedback loop that boosts the expression of BRDs in order to increase AR chromatin accessibility. Moreover, ATAD2 had strong prognostic value on a cohort of 10,000 patients. Our data also suggest that, while ATAD2 is an optimal tissue biomarker in identifying PC tissues where active transcription due to heavy cell-cycle turnover is ongoing, it may not be a good target for PC therapy, as also shown recently (Bamborough et al., 2016), if not targeted in combination with other agents such as antiandrogens.

The role of ATAD2 as a regulator of chromatin dynamics is well known in yeast (Cattaneo et al., 2014). A recent study showed that ATAD2 is highly expressed in replicating PC cells and ATAD2 expression correlates with expression of cell-cycle and DNA replication genes that have overlapping function in meiosis and tumor progression (Koo et al., 2016). Moreover, in highly proliferating embryonic stem cells, ATAD2 was reported to sustain specific gene expression programs via regulating chromatin opening guided by histone acetylation (Morozumi et al., 2016), which is in agreement with our data. These findings corroborate our data and are supportive of ATAD2 being a possible contributor to increased transcription plasticity in CRPC.

Our study also suggests that there might be a subpopulation of tumors that are more dependent on BRDs activity than others. Therefore, we built a ten-gene signature, BROMO-10, which is able to discriminate patients with poorer outcome, which takes into account chromatin structure and additionally incorporates key PC-specific downstream targets of BRDs. Interestingly, these targets include *FEN1*, which we have previously described to be important for PC progression and proposed as a tissue biomarker for biochemical recurrence (Urbanucci et al., 2012b), EEF1A2, which has been proposed as a marker of prostate cell transformation (Scaggiante et al., 2012; Sun et al., 2014), *KAT2A*, which encodes a histone acetyl-transferase controlling the PI3/AKT pathway with therapeutic potential in leukemia (Sun et al., 2015), and *HSPH1*, which enhances MYC transcription and drives B cell non-Hodgkin lymphoma (Zappasodi et al., 2015).

Mechanisms of resistance to BET inhibition have been reported. Therefore, it is extremely important to define patients that will respond to BET-inhibition therapies in combination with standard therapies to avoid resistance. We show that BROMO-10 is able to predict response to BET-inhibition therapies, but the use of this signature should be limited to tumors with intact AR signaling, and further studies are needed to refine the signature for different compounds.

In conclusion, we propose AR deregulation-driven chromatin structure as a key determinant of tumor progression. We describe the effect of BET inhibition on chromatin accessibility as an additional mechanism by which it is able to repress cell growth in a cell-specific manner. Moreover, we propose BROMO-10 signature to be used to select patients more likely to benefit from BET-targeted therapies and avoid recurrence. The selection of PC patients into future trials evaluating the efficacy should be based on the assessment of AR status, key BRDs expression, such as ATAD2, and the gene signature that reflects the chromatin status of these tumors.

EXPERIMENTAL PROCEDURES

Clinical Samples

All work on clinical samples has been carried out in compliance with the Helsinki Declaration and with the approval of ethics boards at collaborating institutions as outlined below. The tissue microarray from the Department of Urology and the Martini Clinics at the University Medical Centre Hamburg-Eppendorf consisted of archived diagnostic leftover tissues. Manufacture and analysis was approved by the local ethics committee (Ethics commission Hamburg, WF-049/09 and PV3652). According to local laws (HmbKHG, §12,1), informed consent was not required for this study. Patient records and information were anonymized and de-identified prior to analysis.

Three BPH, six primary PC, and three CRPCs were used for FAIRE-seq assays and FAIRE-qPCR assays. RNA-seq data from transcriptomes of 12 BPH, 28 untreated PCs, and 13 CRPCs, including the samples used for FAIRE-seq, were publicly available (Ylipää et al., 2015). These samples and the tissue

microarray described below were provided by Tampere University Hospital. The use of these samples for FAIRE-seq and of the tissue microarray was approved by the ethical committee of Tampere University Hospital and the National Authority for Medicolegal Affairs. Written informed consent was obtained from the subjects for sequencing the samples.

The Tampere patients' cohort of tissue microarrays (TMAs) contained 258 formalin-fixed paraffin-embedded prostatectomy and 121 CRPC specimens. A subset of the cohort was used to immunostain for ATAD2, BRD2, and BRD4. The Hamburg patients' TMA cohort contained 9,467 prostatectomy tissue specimens. Radical prostatectomy specimens were available from 12,427 patients. PSA values were measured following surgery, and PSA recurrence was defined as the time point when postoperative PSA was increasing from at least 0.2 ng/mL.

FAIREs

Two replicates were processed for each cell line and condition for subsequent sequencing analysis. Three to five replicates were processed for qPCR analysis. Four million cells were plated and hormone deprived for 4 days. Cells were then treated with R1881 or DHT for 4 hr. To perform tissue FAIRE from clinical material, 3 mL of PBS containing 2 × protease inhibitor (Roche) was added to 40 × 20-μm sections of freshly frozen tissue specimens. Downstream fixation and processing of both sample types are as described in the Supplemental Information.

FAIRE-Seq Analysis

Peak detection for FAIRE-seq was performed using model-based analysis of ChIP-seq (MACS) (Zhang et al., 2008) with default parameters using inputs of each of the FAIRE samples as controls and with F-Seq (Boyle et al., 2008). Refer to Supplemental Information for more detail.

Evaluation of the 15-Gene Signature Prognostic Value

Microarray data from the Decipher GRID were extracted for three radical prostatectomy cohorts from previously described (Erho et al., 2013; Karnes et al., 2013; Ross et al., 2016) validation studies. A classifier to distinguish between metastatic versus non-metastatic cancers was developed. The classifier was constructed from 15 genes (Figure 5C) using a generalized linear model with elastic net regularization as previously described (Erho et al., 2013). The model was generated using the MCI cohort (GSE46691) as training data. In the final model, ten of the 15 genes contributed to the model score with six positively associated and four negatively associated genes as determined by the regularized coefficients (see also Table S6). Scores were then generated for samples from the Mayo Clinic II (MCII) and JHMI-RP validation cohorts, and performance in each cohort was assessed using survival analysis.

BROMO-10 scores in cell lines and patients derived xenografts were calculated using GSVA Bioconductor package (https://www.bioconductor.org/packages/release/bioc/html/GSVA.html).

Statistics

Statistical analyses were performed using GraphPad Prism, MATLAB, and Microsoft Excel. All statistical tests were two-tailed with testing level thresholds of $\alpha = 0.05$.

ACCESSION NUMBERS

The accession number for the gene expression and FAIRE-seq data reported in this paper is GEO: GSE73989. The data analysis script referred to in the Supplementary Experimental Procedures has also been deposited and is accessible at https://github.com/dvbcfo/depth_track_window.

SUPPLEMENTAL INFORMATION

Supplemental Information includes six figures, six tables, and one data file and can be found with this article online at http://dx.doi.org/10.1016/j.celrep.2017.05.049.

AUTHOR CONTRIBUTIONS

A.U. wrote the manuscript. I.G.M. and A.U. designed the study and analyzed the data. A.U., T.T., S.M., C.B., K.K.K., X.S., and S.J.B. performed experiments and edited the manuscript. A.U., V.K., D.V., M.T., M.A., E.D., I.M.C., P.L., and N.E. performed the bioinformatic analyses and edited the manuscript. H.M.I., A.K., and F.S. assisted in the preparation of the revised manuscript. D.J.V.G., S. Knapp, S. Kregel, R.J.K., A.E.R., P.S.N., E.C., F.Y.F., E.M.S., K.E.K., and M.N. contributed reagents or data and edited the manuscript. G.S., T.S., and T.L.J.T. provided clinical material and edited the manuscript. I.M., T.V., and L.S. contributed reagents and edited the manuscript.

ACKNOWLEDGMENTS

We thank Ms. Päivi Martikainen for the skillful technical assistance. We acknowledge the last scientific contribution of our beloved Ms. Mariitta Vakkuri to this work. A.U. is supported by the South-East Norway Health Authorities (Helse Sor-Ost grant ID 2014040) at the Oslo University Hospital and the Norwegian Centre for Molecular Medicine. I.M. has been funded by the MLS (390000 and 143295), Helse Sor-Ost (2014040), Norwegian Research Council (230559), and the Faculty of Medicine at the Oslo University Hospital. P.S.N., E.C., and I.M.C. are supported by NIH grants P50CA097186 and P01CA163227, and the Prostate Cancer Foundation. H.M.I. is supported by the Norwegian Cancer Society (711072, 102032, and 4521627). S. Knapp is grateful for support by the SGC, a registered charity (number 1097737) that receives funds from AbbVie, Bayer Pharma AG, Boehringer Ingelheim, Canada Foundation for Innovation, Eshelman Institute for Innovation, Genome Canada, Innovative Medicines Initiative (EU/EFPIA), Janssen, Merck & Co., Novartis Pharma AG, Ontario Ministry of Economic Development and Innovation, Pfizer, São Paulo Research Foundation-FAPESP, Takeda, and the Wellcome Trust. The funders had no role in the study design, data collection and analysis, the decision to publish, or preparation of the article.

Received: September 11, 2016
Revised: April 1, 2017
Accepted: May 12, 2017
Published: June 6, 2017

REFERENCES

Andreu-Vieyra, C., Lai, J., Berman, B.P., Frenkel, B., Jia, L., Jones, P.A., and Coetzee, G.A. (2011). Dynamic nucleosome-depleted regions at androgen receptor enhancers in the absence of ligand in prostate cancer cells. Mol. Cell. Biol. *31*, 4648–4662.

Asangani, I.A., Dommeti, V.L., Wang, X., Malik, R., Cieslik, M., Yang, R., Escara-Wilke, J., Wilder-Romans, K., Dhanireddy, S., Engelke, C., et al. (2014). Therapeutic targeting of BET bromodomain proteins in castration-resistant prostate cancer. Nature *510*, 278–282.

Asangani, I.A., Wilder-Romans, K., Dommeti, V.L., Krishnamurthy, P.M., Apel, I.J., Escara-Wilke, J., Plymate, S.R., Navone, N.M., Wang, S., Feng, F.Y., and Chinnaiyan, A.M. (2016). BET bromodomain inhibitors enhance efficacy and disrupt resistance to AR antagonists in the treatment of prostate cancer. Mol. Cancer Res. *14*, 324–331.

Attwell, S., Jahagirdar, R., Norek, K., Calosing, C., Tsujikawa, L., Kharenko, O.A., Patel, R.G., Gesner, E.M., Corey, E., Nguyen, H.M., et al. (2016). Abstract LB-207: Preclinical characterization of ZEN-3694, a novel BET bromodomain inhibitor entering phase I studies for metastatic castration-resistant prostate cancer (mCRPC). Cancer Res. *76*, LB-207–LB-207.

Bamborough, P., Chung, C.W., Demont, E.H., Furze, R.C., Bannister, A.J., Che, K.H., Diallo, H., Douault, C., Grandi, P., Kouzarides, T., et al. (2016). A chemical probe for the ATAD2 bromodomain. Angew. Chem. Int. Ed. Engl. *55*, 11382–11386.

Boyle, A.P., Guinney, J., Crawford, G.E., and Furey, T.S. (2008). F-Seq: A feature density estimator for high-throughput sequence tags. Bioinformatics *24*, 2537–2538.

Buttigliero, C., Tucci, M., Bertaglia, V., Vignani, F., Bironzo, P., Di Maio, M., and Scagliotti, G.V. (2015). Understanding and overcoming the mechanisms of primary and acquired resistance to abiraterone and enzalutamide in castration resistant prostate cancer. Cancer Treat. Rev. *41*, 884–892.

Cattaneo, M., Morozumi, Y., Perazza, D., Boussouar, F., Jamshidikia, M., Rousseaux, S., Verdel, A., and Khochbin, S. (2014). Lessons from yeast on emerging roles of the ATAD2 protein family in gene regulation and genome organization. Mol. Cells *37*, 851–856.

Cedar, H., and Bergman, Y. (2012). Programming of DNA methylation patterns. Annu. Rev. Biochem. *81*, 97–117.

Center, M.M., Jemal, A., Lortet-Tieulent, J., Ward, E., Ferlay, J., Brawley, O., and Bray, F. (2012). International variation in prostate cancer incidence and mortality rates. Eur. Urol. *61*, 1079–1092.

Chen, Z., Lan, X., Thomas-Ahner, J.M., Wu, D., Liu, X., Ye, Z., Wang, L., Sunkel, B., Grenade, C., Chen, J., et al. (2015). Agonist and antagonist switch DNA motifs recognized by human androgen receptor in prostate cancer. EMBO J. *34*, 502–516.

Delmore, J.E., Issa, G.C., Lemieux, M.E., Rahl, P.B., Shi, J., Jacobs, H.M., Kastritis, E., Gilpatrick, T., Paranal, R.M., Qi, J., et al. (2011). BET bromodomain inhibition as a therapeutic strategy to target c-Myc. Cell *146*, 904–917.

Dolfini, D., and Mantovani, R. (2013). Targeting the Y/CCAAT box in cancer: YB-1 (YBX1) or NF-Y? Cell Death Differ. *20*, 676–685.

Erho, N., Crisan, A., Vergara, I.A., Mitra, A.P., Ghadessi, M., Buerki, C., Bergstralh, E.J., Kollmeyer, T., Fink, S., Haddad, Z., et al. (2013). Discovery and validation of a prostate cancer genomic classifier that predicts early metastasis following radical prostatectomy. PLoS ONE *8*, e66855.

Erzurumlu, Y., and Ballar, P. (2017). Androgen mediated regulation of endoplasmic reticulum-associated degradation and its effects on prostate cancer. Sci. Rep. *7*, 40719.

Filippakopoulos, P., and Knapp, S. (2014). Targeting bromodomains: Epigenetic readers of lysine acetylation. Nat. Rev. Drug Discov. *13*, 337–356.

Filippakopoulos, P., Picaud, S., Mangos, M., Keates, T., Lambert, J.P., Barsyte-Lovejoy, D., Felletar, I., Volkmer, R., Müller, S., Pawson, T., et al. (2012). Histone recognition and large-scale structural analysis of the human bromodomain family. Cell *149*, 214–231.

Fu, L.L., Tian, M., Li, X., Li, J.J., Huang, J., Ouyang, L., Zhang, Y., and Liu, B. (2015). Inhibition of BET bromodomains as a therapeutic strategy for cancer drug discovery. Oncotarget *6*, 5501–5516.

Giresi, P.G., and Lieb, J.D. (2009). Isolation of active regulatory elements from eukaryotic chromatin using FAIRE (formaldehyde assisted isolation of regulatory elements). Methods *48*, 233–239.

He, H.H., Meyer, C.A., Shin, H., Bailey, S.T., Wei, G., Wang, Q., Zhang, Y., Xu, K., Ni, M., Lupien, M., et al. (2010). Nucleosome dynamics define transcriptional enhancers. Nat. Genet. *42*, 343–347.

Karnes, R.J., Bergstralh, E.J., Davicioni, E., Ghadessi, M., Buerki, C., Mitra, A.P., Crisan, A., Erho, N., Vergara, I.A., Lam, L.L., et al. (2013). Validation of a genomic classifier that predicts metastasis following radical prostatectomy in an at risk patient population. J. Urol. *190*, 2047–2053.

Koo, S.J., Fernández-Montalván, A.E., Badock, V., Ott, C.J., Holton, S.J., von Ahsen, O., Toedling, J., Vittori, S., Bradner, J.E., and Gorjánácz, M. (2016). ATAD2 is an epigenetic reader of newly synthesized histone marks during DNA replication. Oncotarget *7*, 70323–70335.

Kregel, S., Kiriluk, K.J., Rosen, A.M., Cai, Y., Reyes, E.E., Otto, K.B., Tom, W., Paner, G.P., Szmulewitz, R.Z., and Vander Griend, D.J. (2013). Sox2 is an androgen receptor-repressed gene that promotes castration-resistant prostate cancer. PLoS ONE *8*, e53701.

Kumar, A., Coleman, I., Morrissey, C., Zhang, X., True, L.D., Gulati, R., Etzioni, R., Bolouri, H., Montgomery, B., White, T., et al. (2016). Substantial interindividual and limited intraindividual genomic diversity among tumors from men with metastatic prostate cancer. Nat. Med. *22*, 369–378.

Lever, E., and Sheer, D. (2010). The role of nuclear organization in cancer. J. Pathol. *220*, 114–125.

Lovén, J., Hoke, H.A., Lin, C.Y., Lau, A., Orlando, D.A., Vakoc, C.R., Bradner, J.E., Lee, T.I., and Young, R.A. (2013). Selective inhibition of tumor oncogenes by disruption of super-enhancers. Cell *153*, 320–334.

Massie, C.E., Lynch, A., Ramos-Montoya, A., Boren, J., Stark, R., Fazli, L., Warren, A., Scott, H., Madhu, B., Sharma, N., et al. (2011). The androgen receptor fuels prostate cancer by regulating central metabolism and biosynthesis. EMBO J. *30*, 2719–2733.

Morozumi, Y., Boussouar, F., Tan, M., Chaikuad, A., Jamshidikia, M., Colak, G., He, H., Nie, L., Petosa, C., de Dieuleveult, M., et al. (2016). Atad2 is a generalist facilitator of chromatin dynamics in embryonic stem cells. J. Mol. Cell Biol. *8*, 349–362.

Nagarajan, S., Hossan, T., Alawi, M., Najafova, Z., Indenbirken, D., Bedi, U., Taipaleenmäki, H., Ben-Batalla, I., Scheller, M., Loges, S., et al. (2014). Bromodomain protein BRD4 is required for estrogen receptor-dependent enhancer activation and gene transcription. Cell Rep. *8*, 460–469.

Nguyen, H.M., Vessella, R.L., Morrissey, C., Brown, L.G., Coleman, I.M., Higano, C.S., Mostaghel, E.A., Zhang, X., True, L.D., Lam, H.M., et al. (2017). LuCaP prostate cancer patient-derived xenografts reflect the molecular heterogeneity of advanced disease and serve as models for evaluating cancer therapeutics. Prostate *77*, 654–671.

Perry, A.S., Watson, R.W., Lawler, M., and Hollywood, D. (2010). The epigenome as a therapeutic target in prostate cancer. Nat. Rev. Urol. *7*, 668–680.

Pomerantz, M.M., Li, F., Takeda, D.Y., Lenci, R., Chonkar, A., Chabot, M., Cejas, P., Vazquez, F., Cook, J., Shivdasani, R.A., et al. (2015). The androgen receptor cistrome is extensively reprogrammed in human prostate tumorigenesis. Nat. Genet. *47*, 1346–1351.

Ross, A.E., Johnson, M.H., Yousefi, K., Davicioni, E., Netto, G.J., Marchionni, L., Fedor, H.L., Glavaris, S., Choeurng, V., Buerki, C., et al. (2016). Tissue-based genomics augments post-prostatectomy risk stratification in a natural history cohort of intermediate- and high-risk men. Eur. Urol.

Roudier, M.P., Winters, B.R., Coleman, I., Lam, H.M., Zhang, X., Coleman, R., Chéry, L., True, L.D., Higano, C.S., Montgomery, B., et al. (2016). Characterizing the molecular features of ERG-positive tumors in primary and castration resistant prostate cancer. Prostate *76*, 810–822.

Scaggiante, B., Dapas, B., Bonin, S., Grassi, M., Zennaro, C., Farra, R., Cristiano, L., Siracusano, S., Zanconati, F., Giansante, C., and Grassi, G. (2012). Dissecting the expression of EEF1A1/2 genes in human prostate cancer cells: The potential of EEF1A2 as a hallmark for prostate transformation and progression. Br. J. Cancer *106*, 166–173.

Sharma, N.L., Massie, C.E., Ramos-Montoya, A., Zecchini, V., Scott, H.E., Lamb, A.D., MacArthur, S., Stark, R., Warren, A.Y., Mills, I.G., and Neal, D.E. (2013). The androgen receptor induces a distinct transcriptional program in castration-resistant prostate cancer in man. Cancer Cell *23*, 35–47.

Shi, J., and Vakoc, C.R. (2014). The mechanisms behind the therapeutic activity of BET bromodomain inhibition. Mol. Cell *54*, 728–736.

Song, L., Zhang, Z., Grasfeder, L.L., Boyle, A.P., Giresi, P.G., Lee, B.K., Sheffield, N.C., Gräf, S., Huss, M., Keefe, D., et al. (2011). Open chromatin defined by DNaseI and FAIRE identifies regulatory elements that shape cell-type identity. Genome Res. *21*, 1757–1767.

Stelloo, S., Nevedomskaya, E., van der Poel, H.G., de Jong, J., van Leenders, G.J., Jenster, G., Wessels, L.F., Bergman, A.M., and Zwart, W. (2015). Androgen receptor profiling predicts prostate cancer outcome. EMBO Mol. Med. *7*, 1450–1464.

Sun, Y., Du, C., Wang, B., Zhang, Y., Liu, X., and Ren, G. (2014). Up-regulation of eEF1A2 promotes proliferation and inhibits apoptosis in prostate cancer. Biochem. Biophys. Res. Commun. *450*, 1–6.

Sun, X.J., Man, N., Tan, Y., Nimer, S.D., and Wang, L. (2015). The role of histone acetyltransferases in normal and malignant hematopoiesis. Front. Oncol. *5*, 108.

Tark-Dame, M., Jerabek, H., Manders, E.M., van der Wateren, I.M., Heermann, D.W., and van Driel, R. (2014). Depletion of the chromatin looping proteins CTCF and cohesin causes chromatin compaction: Insight into chromatin folding by polymer modelling. PLoS Comput. Biol. *10*, e1003877.

Taylor, B.S., Schultz, N., Hieronymus, H., Gopalan, A., Xiao, Y., Carver, B.S., Arora, V.K., Kaushik, P., Cerami, E., Reva, B., et al. (2010). Integrative genomic profiling of human prostate cancer. Cancer Cell *18*, 11–22.

Tewari, A.K., Yardimci, G.G., Shibata, Y., Sheffield, N.C., Song, L., Taylor, B.S., Georgiev, S.G., Coetzee, G.A., Ohler, U., Furey, T.S., et al. (2012). Chromatin accessibility reveals insights into androgen receptor activation and transcriptional specificity. Genome Biol. *13*, R88.

Timp, W., and Feinberg, A.P. (2013). Cancer as a dysregulated epigenome allowing cellular growth advantage at the expense of the host. Nat. Rev. Cancer *13*, 497–510.

Urbanucci, A., Marttila, S., Janne, O.A., and Visakorpi, T. (2012a). Androgen receptor overexpression alters binding dynamics of the receptor to chromatin and chromatin structure. Prostate.

Urbanucci, A., Sahu, B., Seppälä, J., Larjo, A., Latonen, L.M., Waltering, K.K., Tammela, T.L., Vessella, R.L., Lähdesmäki, H., Jänne, O.A., and Visakorpi, T. (2012b). Overexpression of androgen receptor enhances the binding of the receptor to the chromatin in prostate cancer. Oncogene *31*, 2153–2163.

Urbanucci, A., Waltering, K., Mills, I., and Visakorpi, T. (2013). The effect of AR overexpression on androgen signaling in prostate cancer. In Androgen-Responsive Genes in Prostate Cancer, Z. Wang, ed. (Springer), pp. 187–200.

Waltering, K.K., Helenius, M.A., Sahu, B., Manni, V., Linja, M.J., Jänne, O.A., and Visakorpi, T. (2009). Increased expression of androgen receptor sensitizes prostate cancer cells to low levels of androgens. Cancer Res. *69*, 8141–8149.

Waltering, K.K., Urbanucci, A., and Visakorpi, T. (2012). Androgen receptor (AR) aberrations in castration-resistant prostate cancer. Mol. Cell. Endocrinol. *360*, 38–43.

Wyce, A., Degenhardt, Y., Bai, Y., Le, B., Korenchuk, S., Crouthamel, M.-C., McHugh, C., Vessella, R., Creasy, C., Tummino, P., et al. (2013). Inhibition of BET bromodomain proteins as a therapeutic approach in prostate cancer. Oncotarget *4*, 2419–2429.

Xu, Y., Dalrymple, S.L., Becker, R.E., Denmeade, S.R., and Isaacs, J.T. (2006). Pharmacologic basis for the enhanced efficacy of dutasteride against prostatic cancers. Clin. Cancer Res. *12*, 4072–4079.

Ylipää, A., Kivinummi, K., Kohvakka, A., Annala, M., Latonen, L., Scaravilli, M., Kartasalo, K., Leppänen, S.P., Karakurt, S., Seppälä, J., et al. (2015). Transcriptome sequencing reveals PCAT5 as a novel ERG-regulated long noncoding RNA in prostate cancer. Cancer Res. *75*, 4026–4031.

Yu, J., Yu, J., Mani, R.S., Cao, Q., Brenner, C.J., Cao, X., Wang, X., Wu, L., Li, J., Hu, M., et al. (2010). An integrated network of androgen receptor, polycomb, and TMPRSS2-ERG gene fusions in prostate cancer progression. Cancer Cell *17*, 443–454.

Zappasodi, R., Ruggiero, G., Guarnotta, C., Tortoreto, M., Tringali, C., Cavanè, A., Cabras, A.D., Castagnoli, L., Venerando, B., Zaffaroni, N., et al. (2015). HSPH1 inhibition downregulates Bcl-6 and c-Myc and hampers the growth of human aggressive B-cell non-Hodgkin lymphoma. Blood *125*, 1768–1771.

Zhang, Y., Liu, T., Meyer, C.A., Eeckhoute, J., Johnson, D.S., Bernstein, B.E., Nusbaum, C., Myers, R.M., Brown, M., Li, W., and Liu, X.S. (2008). Model-based analysis of ChIP-Seq (MACS). Genome Biol. *9*, R137.

Zhang, T.Y., Agarwal, N., Sonpavde, G., DiLorenzo, G., Bellmunt, J., and Vogelzang, N.J. (2013). Management of castrate resistant prostate cancer-recent advances and optimal sequence of treatments. Curr. Urol. Rep. *14*, 174–183.

Zou, J.X., Guo, L., Revenko, A.S., Tepper, C.G., Gemo, A.T., Kung, H.J., and Chen, H.W. (2009). Androgen-induced coactivator ANCCA mediates specific androgen receptor signaling in prostate cancer. Cancer Res. *69*, 3339–3346.

Cell Reports, Volume *19*

Supplemental Information

Androgen Receptor Deregulation Drives Bromodomain-Mediated Chromatin Alterations in Prostate Cancer

Alfonso Urbanucci, Stefan J. Barfeld, Ville Kytölä, Harri M. Itkonen, Ilsa M. Coleman, Daniel Vodák, Liisa Sjöblom, Xia Sheng, Teemu Tolonen, Sarah Minner, Christoph Burdelski, Kati K. Kivinummi, Annika Kohvakka, Steven Kregel, Mandeep Takhar, Mohammed Alshalalfa, Elai Davicioni, Nicholas Erho, Paul Lloyd, R. Jeffrey Karnes, Ashley E. Ross, Edward M. Schaeffer, Donald J. Vander Griend, Stefan Knapp, Eva Corey, Felix Y. Feng, Peter S. Nelson, Fahri Saatcioglu, Karen E. Knudsen, Teuvo L.J. Tammela, Guido Sauter, Thorsten Schlomm, Matti Nykter, Tapio Visakorpi, and Ian G. Mills

Supplementary Figure 1

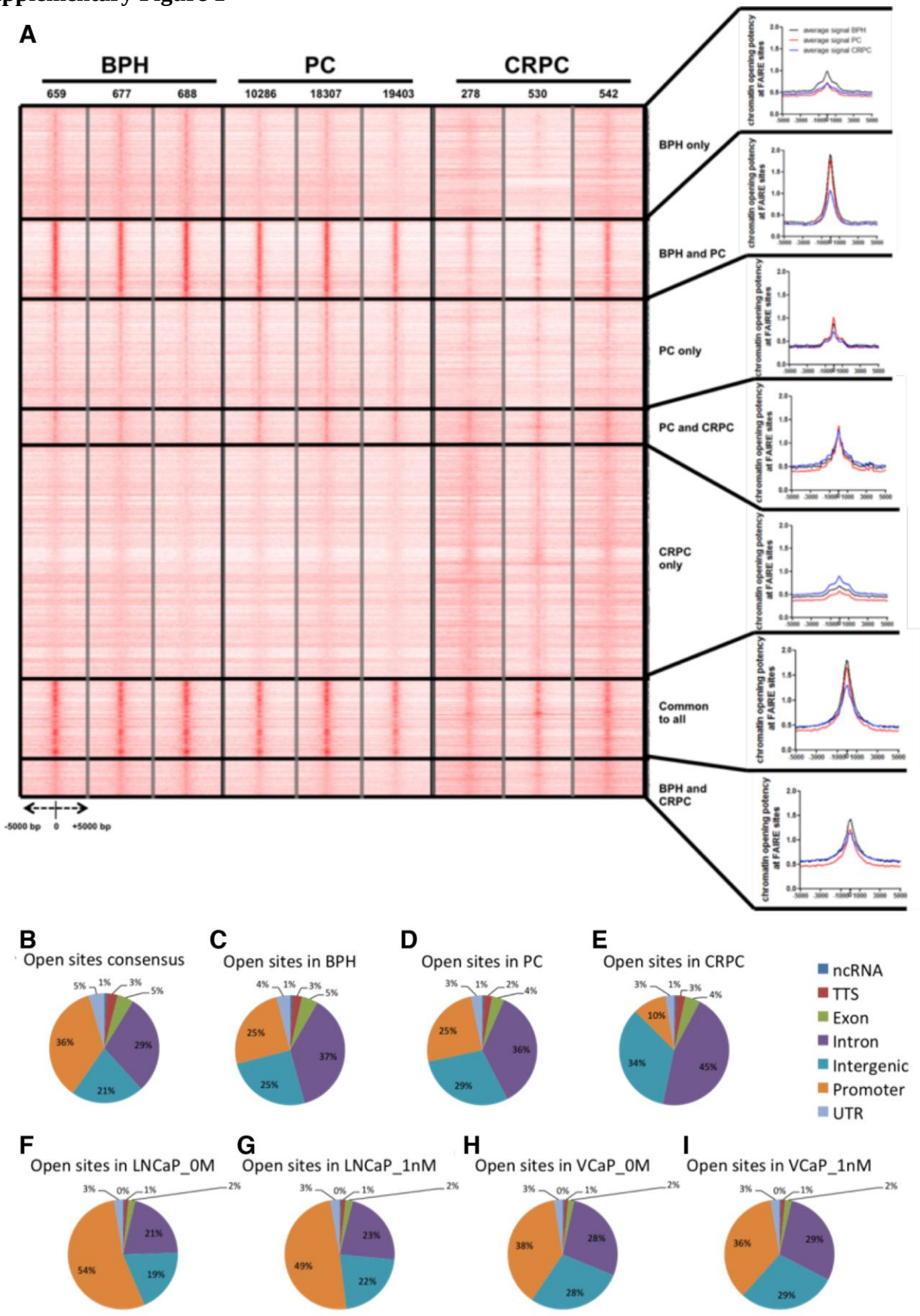

Figure S1. The distribution of FAIRE-seq reads in benign and cancerous prostate tissue samples and their genomic distribution, Related to Figure 1. (A) Formaldehyde–assisted isolation of regulatory elements followed by sequencing (FAIRE-seq) was used to retrieve

accessible genomic regions in tissue specimens from benign prostate hyperplasia (BPH), primary prostate cancer (PC) derived from prostatectomy and locally recurrent castration resistant prostate cancer (CRPC) from transurethral resection of the prostate. Only high confidence open chromatin regions in 3 BPH (23574 sites), 3 primary PC (23341 sites), and 3 CRPC (29160 sites) tissue samples were considered in this analysis. Overlapping and unique peak centres (as indicated on the left) were used to assess distribution of FAIRE-seq reads in the three tissue samples types around these sites (+-5000bp from the centre). Average read distribution was assessed for each category (BPH, PC, and CRPC) of FAIRE-seq peaks and is indicated in the line charts on the right side of the figure. Distribution of common chromatin open sites in all 9 clinical tissue samples (**B**), in all benign prostate hyperplasia (BPH) samples (**C**), in all primary prostate cancer (PC) tissue samples (**D**), and in all castration resistant prostate cancer tissue samples (**E**) according to FAIRE-seq analysis. Distribution of chromatin open sites in LNCaP (**F&G**) and VCaP (**H&I**) cells treated with vehicle (**F&H**) or 1 nM R1881 for 4 hours (**G&I**) following three days of hormone starvation prior to the FAIRE-seq assay.

Supplementary Figure 2

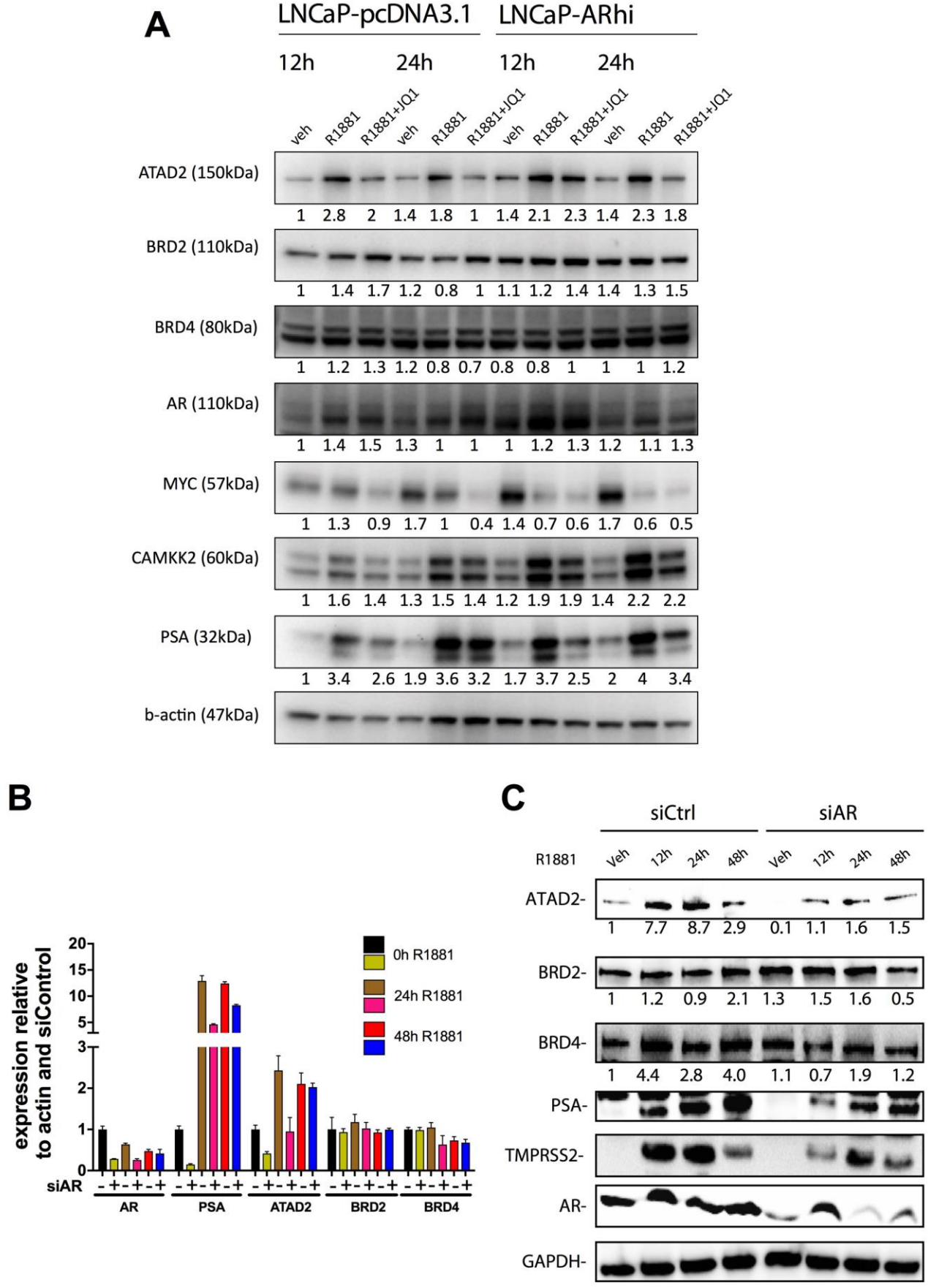

Figure S2. Bromodomain containing protein regulation by androgens, Related to Figure 3. (**A**) Western blot analysis of ATAD2, BRD2, BRD4, AR, MYC, CAMKK2, and PSA in LNCaP-pcDN3.1 and LNCaP-ARhi (LNCaP ARhi) cells 12 and 24 hours after treatment with vehicle (veh

= ethanol), 1nM synthetic androgen R1881 or 1 nM R1881 and 125 nM JQ1. Quantity One software was used to measure the intensity of bands as indicated. β-actin and LNCaP-pcDNA3.1 cells treated for 12 hours with vehicle was used as the point of normalization. Indicated genes' qRT-PCR (**B**) and Western blot analysis (**C**) in LNCaP reverse transfected with either control or siRNA against AR. The cells were hormone starved for 2 days before the treatment with 1 nM R1881 for the indicated time points. Ratio values relative to siControl and are shown for ATAD2, BRD2, and BRD4 blots. TMPRSS2, PSA, and AR levels are shown as control.

Supplementary Figures 3A-H

A

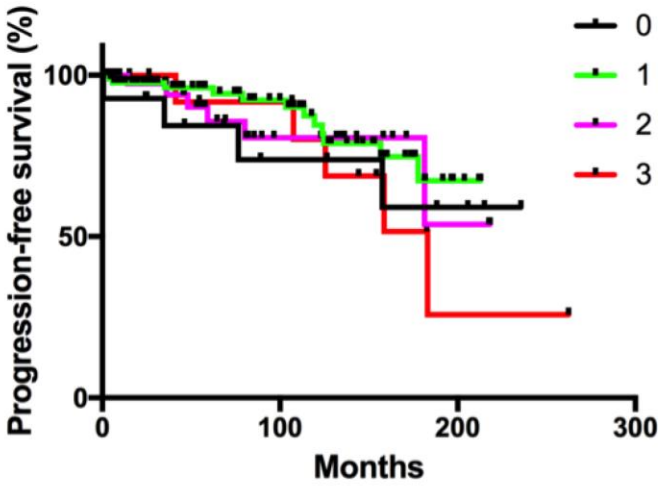

B

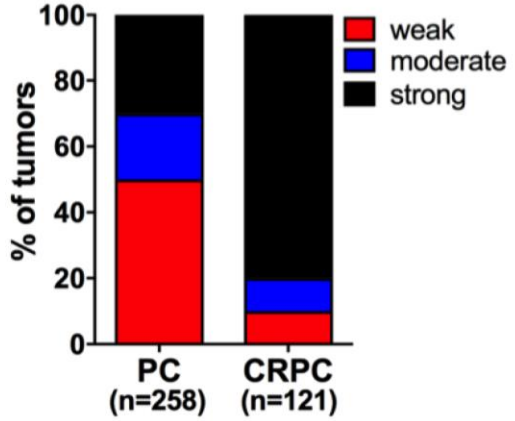

C

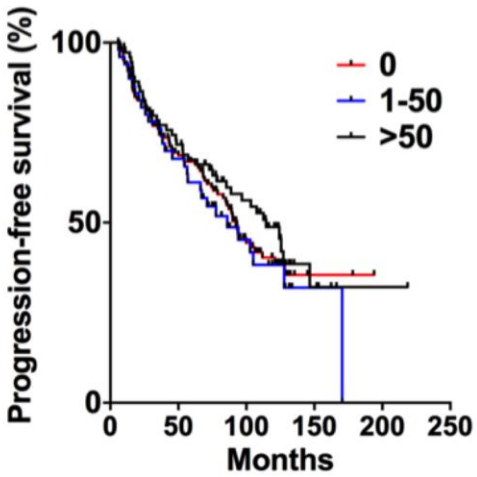

D

Variable	ATAD2 cytoplasmic histoscore			P	ATAD2 % of positive nuclei			P
	0	1-50	51-300		0	1-5	>5	
Prostatectomy specimens, n (%)	129 (50)	52 (20)	77 (30)		169 (66)	83 (32)	6 (2)	
Locally recurrent CRPCs, n (%)	12 (10)	12 (10)	97 (80)	<0.0001	39(32)	38 (32)	43 (36)	<0.0001
Prostatectomy specimens:								
Gleason score, n (%)								
<7	51 (53)	16 (17)	29 (30)		73 (76)	23 (24)	0 (0)	
7	61 (49)	28 (23)	35 (28)		76 (61)	44 (36)	4 (3)	
>7	17 (49)	7 (20)	11(31)	0.866	20 (57)	13 (37)	2 (6)	0.053
pT-stage, n (%)								
pT2	84 (47)	37 (21)	56 (32)		121 (68)	55 (31)	1 (1)	
pT3	45 (56)	15 (19)	20 (25)	0.407	48 (60)	27 (34)	5 (6)	0.015
PSA ng/ml (mean ± SD)	18.1 ± 25.4	12.8 ± 9.4	12.4 ± 8.4	0.091	16.3 ± 22.1	12.9 ± 9.2	17.0 ± 10.0	0.423
Age (mean ± SD)	63.0 ± 4.9	64.3± 4.8	62.3 ± 5.8	0.125	63.4 ± 4.9	62.2 ± 5.8	63.8 ± 5.8	0.288

E F G H

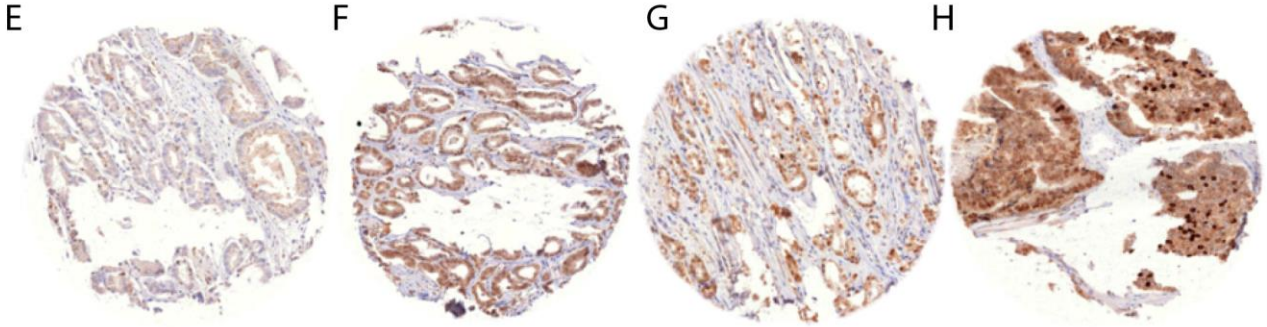

Supplementary Figures 3I-M

I

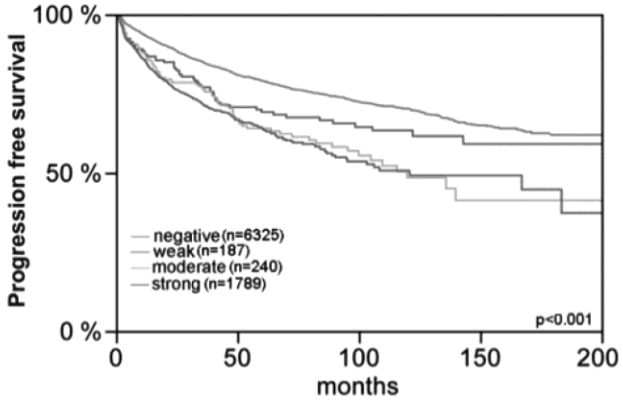

J

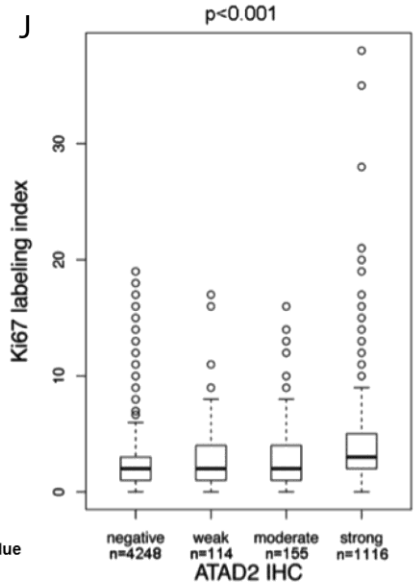

K

Parameter	ATAD2				n evaluable	p value
	negative (%)	weak (%)	moderate (%)	strong (%)		
All cancers	73,7	2,2	2,8	21,3	9467	
Tumor stage						<0.0001
pT2	78,1	1,8	2,3	17,7	6085	
pT3a	68,7	2,8	3,2	25,3	2111	
pT3b	60,3	2,9	4,2	32,7	1179	
pT4	55,6	1,9	13,0	29,6	54	
Gleason grade						<0.0001
≤3+3	86,4	2,2	2,1	9,3	2141	
3+4	74,6	1,9	2,4	21,0	5368	
4+3	59,4	2,9	4,3	33,4	1451	
≥4+4	48,5	2,6	5,9	43,0	460	
Lymph node metastasis						<0.0001
N0	71,2	2,2	2,9	23,7	5460	
N+	56,3	2,0	3,3	38,4	549	
Preop. PSA level (ng/ml)						0.0006
<4	75,9	1,6	2,8	19,7	1154	
4-10	74,4	1,9	2,5	21,2	5665	
10-20	71,0	3,1	3,1	22,8	1878	
>20	69,7	3,3	4,2	22,9	669	
Surgical margin						0.0005
negative	74,7	2,2	2,8	20,3	7495	
positive	70,4	2,2	2,6	24,8	1799	

L

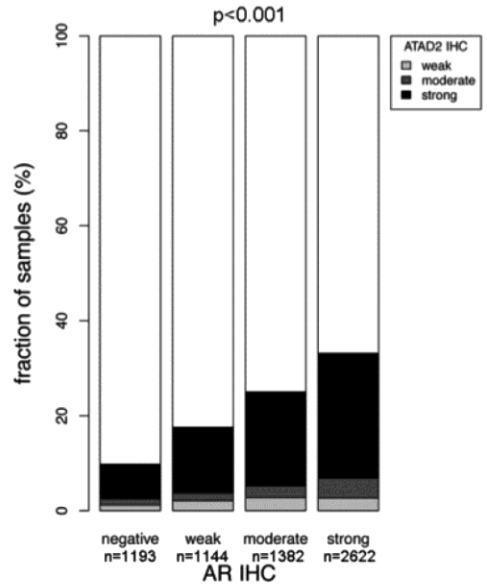

M

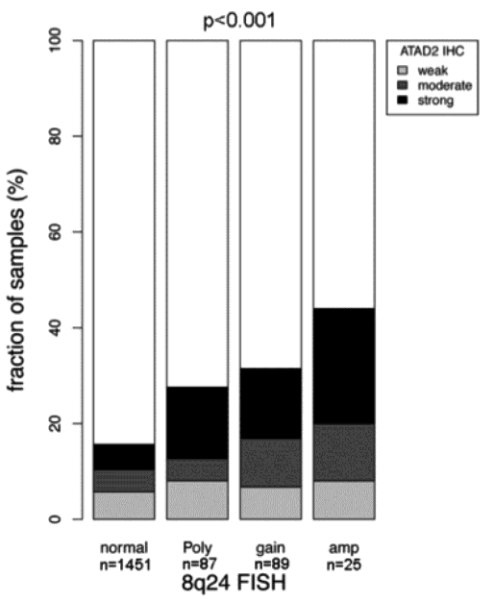

Figure S3. Immunohistochemical analysis of bromodomain containing proteins in two prostate cancer cohorts (Tampere and Hamburg) related to Figure 4. BRD4 (**A** and **B**) and ATAD2 (**C** and **D**) analyses in the Tampere cohort. (**A**) Kaplan–Meier analysis of biochemical progression-free survival in 159 prostatectomy-treated patients according to BRD4 long isoform staining. (**B**) Percentage of tumors according to ATAD2 cytoplasmic histoscore in PC (n=258) and CRPC (n=121) specimens ($p<0.0001$ according to X^2 test). (**C**) Kaplan–Meier analysis of biochemical progression-free survival in prostatectomy-treated patients according to ATAD2 cytoplasmic histoscore ($p=0.5234$ calculated with Mantel–Cox test). (**D**) Association of ATAD2 cytoplasmic histoscore and ATAD2 percentage of positive nuclei with Gleason Score, pT stage, PSA testing, and age. Analysis of ATAD2 in prostate cancer in Hamburg validation cohort;staining intensity of all prostate cancer cases was semi-quantitatively assessed in four categories for which representative images are given: (**E**) negative, (**F**) weak, (**G**) moderate, and (**H**) strong. (**I**). Kaplan–Meier analysis of biochemical progression-free survival in the Hamburg validation cohort of 8541 prostatectomy-treated patients according to ATAD2 staining.Association between ATAD2 immunostaining intensity and Ki67 index label (**J**). (**K**) Association between ATAD2 immunostaining results and prostate cancer phenotype in all cancers. Percentage of tumors that co-stained for androgen receptor (AR) and ATAD2 ($p<0.001$ according to X^2 test) (**L**), and were positive for 8q24 locus (ATAD2 locus) alteration as assessed by fluorescence in situ hybridization (FISH) ($p=0.0009$) (**M**).

Supplementary Figure 4

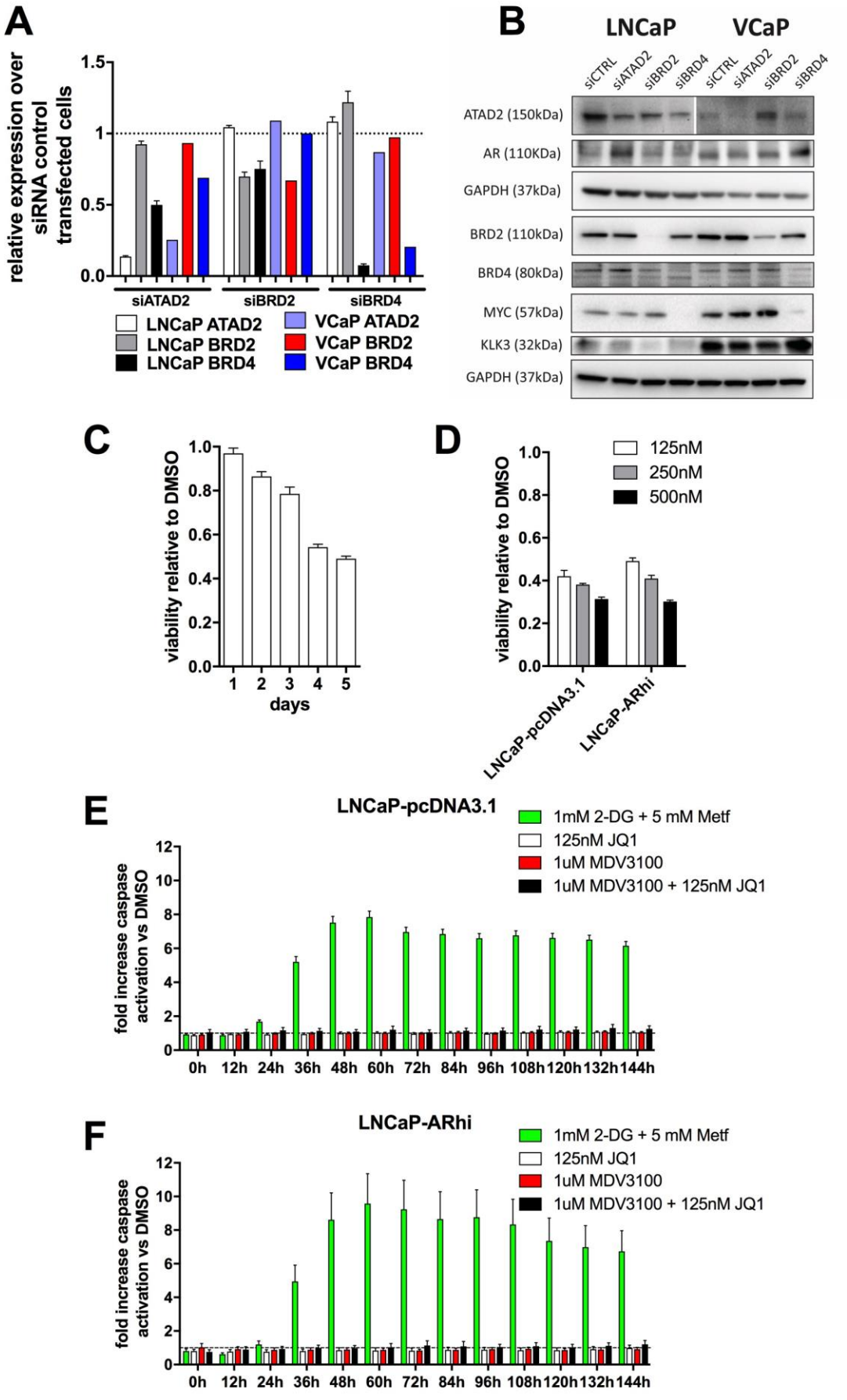

Figure S4. Impact of bromodomain inhibition on androgen receptor positive prostate cancer cells, Related to Figure 5. (**A**) qPCR analysis of ATAD2, BRD2, and BRD4 transcripts in LNCaP

and VCaP cells three days after transfection with siRNA control or siRNA against ATAD2 (siATAD2), siRNA against BRD2 (siBRD2), or siRNA against BRD4 (siBRD4). The relative expression of each gene normalized against house-keeping gene and normalization against the relative siRNA control value are shown. (**B**) Western blot analysis of ATAD2, BRD2, and BRD4 proteins knockdown in LNCaP and VCaP cells following three days transfection with the indicated siRNAs. Protein levels of AR, PSA (KLK3), and MYC are also shown. (**C**) Relative viability of 22RV1 cells cultured in full serum and treated with DMSO or 125 nM bromodomain inhibitor JQ1 for the indicated time. (**D**) Relative viability of LNCaP-pcDNA3.1 cells and AR overexpressing LNCaP-ARhi cells cultured in full serum and treated for 96 hours with the indicated concentrations of JQ1. Caspase activation assay following a time course treatment of 2-deoxy-glucose (2-DG) supplemented with metformin (Metf) to induce caspase activation as positive control, JQ1, MDV3100 or the combination of the last two (indicated concentrations) in LNCaP-pcDNA3.1 (**E**) and LNCaP-ARhi (**F**) cells

Supplementary Figures 5A-D

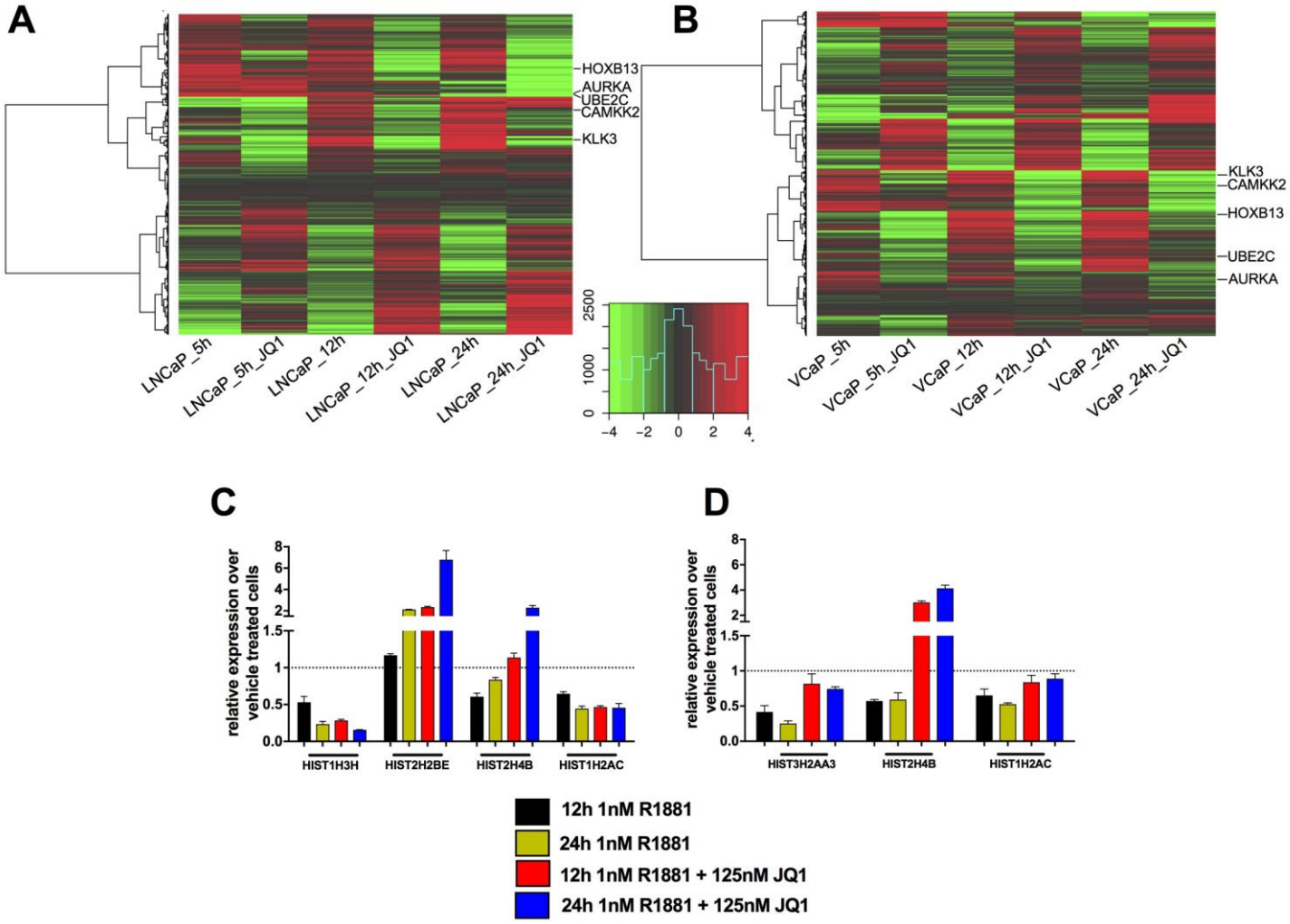

Supplementary Figures 5 E-J

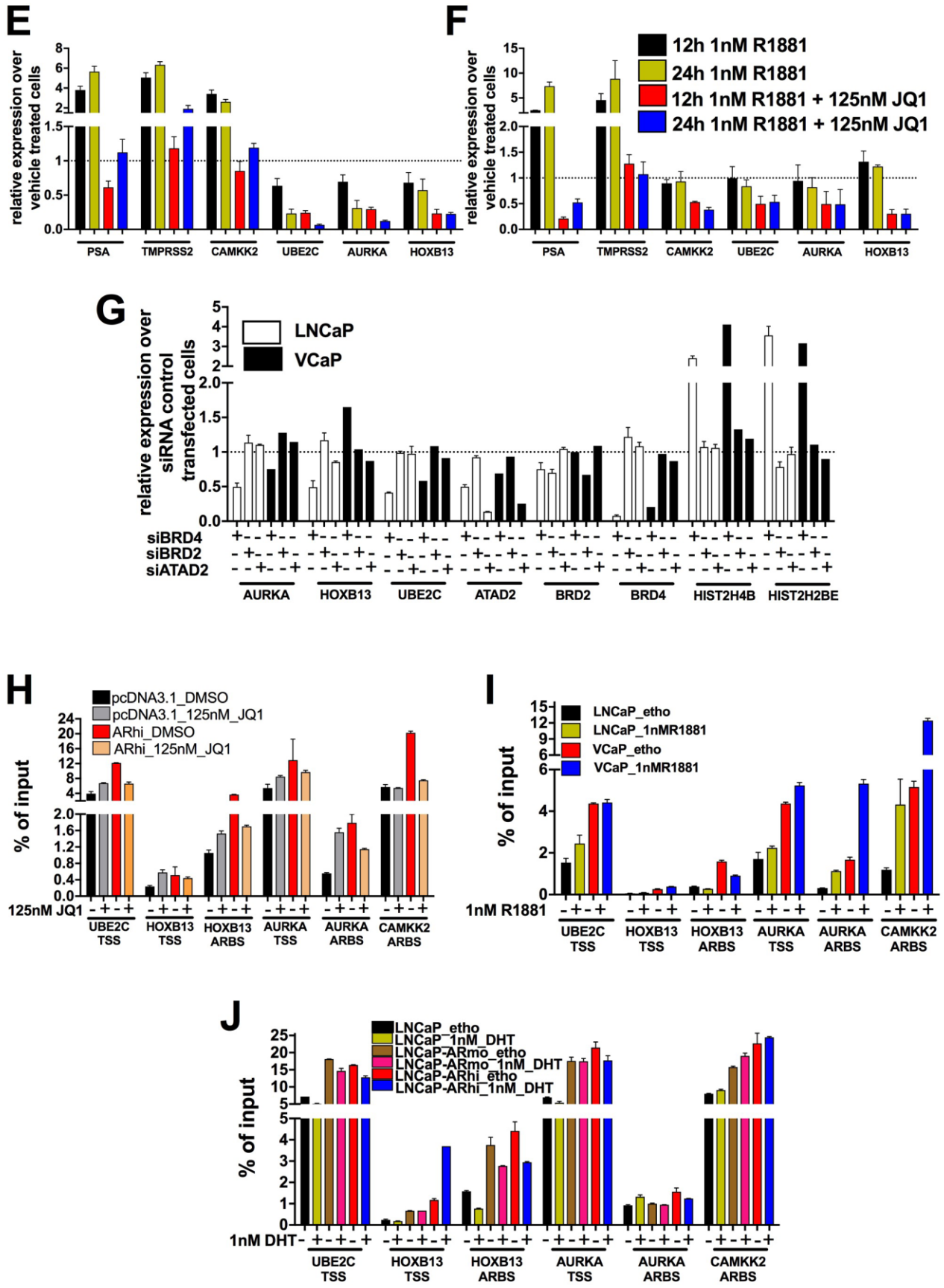

Figure S5. **Impact of JQ1 on the transcriptional program of prostate cancer cells shows downregulation of key androgen receptor target genes and upregulation of histone genes, Related to Figure 6.** Heat maps of genes up- and down-regulated by JQ1 in LNCaP (**A**) and VCaP

(**B**) cells. qRT-PCR validation of micro array data showing upregulation of the indicated histone genes in LNCaP (**C**) and VCaP (**D**) cells upon treatment with JQ1 for the indicated time. qRT-PCR validation of micro array data showing downregulation of the indicated genes in LNCaP (**E**) and VCaP (**F**) cells upon treatment with JQ1 for the indicated time, or upon knockdown of the indicated bromodomains (**G**). Two histone genes also show upregulation upon BRD4 knockdown. Validated FAIRE-seq sites by FAIRE-qPCR analysis (**H-J**). Cells were assayed via FAIRE-qPCR following four days of hormone starvation, in two cases with concomitant treatment with subtoxic concentration of 125 nM small molecule bromodomain inhibitor JQ1 or vehicle (DMSO) (**H**). FAIRE-qPCR validation of local chromatin opening at the indicated loci in LNCaP and VCaP cells treated for 4h with 1 nM R1881 or vehicle (etho) after three days of hormone starvation (**I**) and in a LNCaP-based AR overexpression model (described in Waltering et al.(Waltering et al., 2009)) treated for 4 hours with dihydrotestosterone (DHT) or vehicle (etho) following three days of hormone starvation (**J**).

Supplementary Figures 6A-C

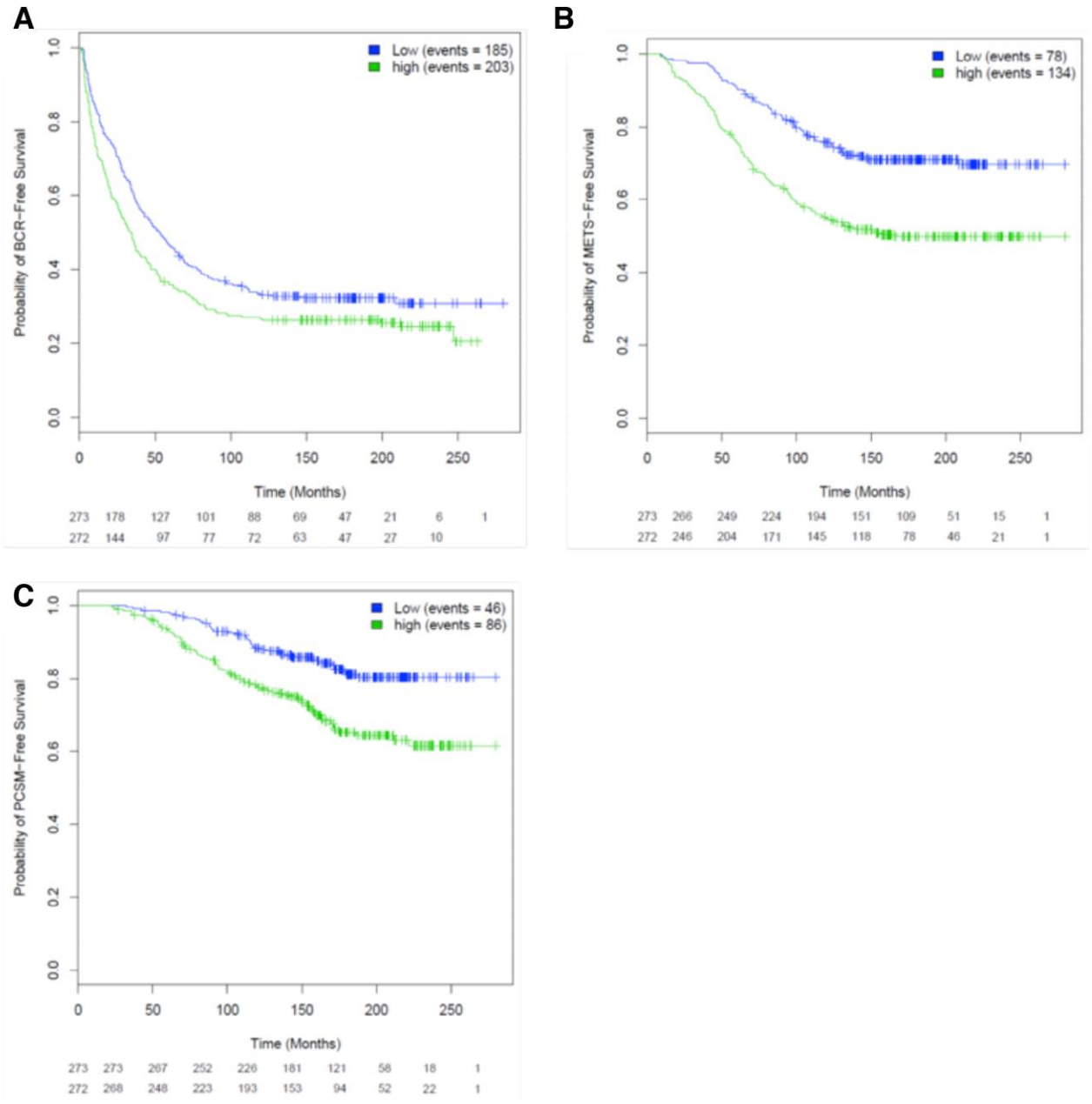

Supplementary Figures 6D-G

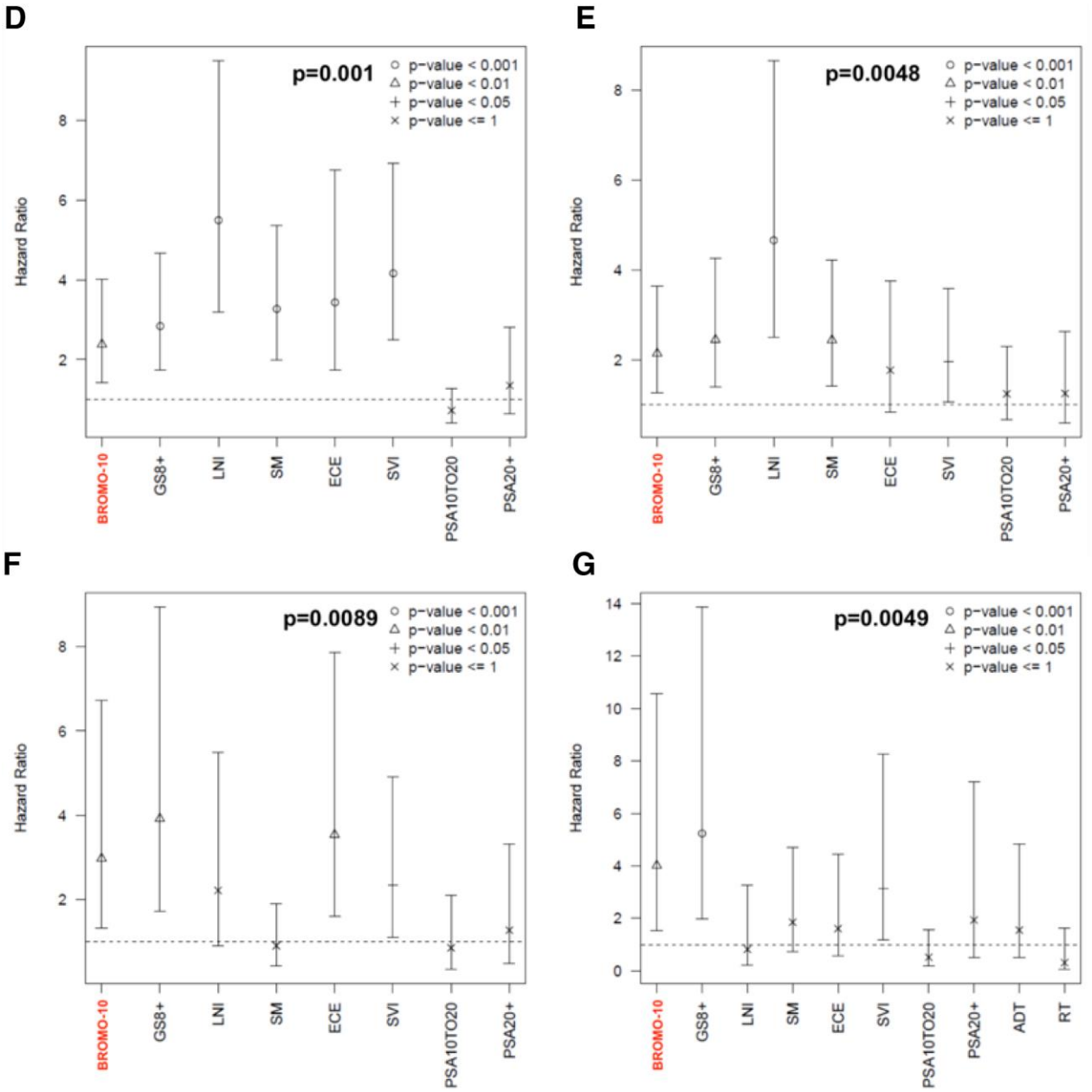

Figure S6. Evaluating the predictive value and independent prognostic contribution of the BROMO-10 signature. Related to Figure 7. Predictive values for the 10 genes in the signature in the MCI cohort of high-risk men, Kaplan-Meier survival curves show (**A**) biochemical recurrence (BCR) -free survival (p=0.00935), (**B**) Metastatic recurrence (METS) -free survival (p=0.0000001), and (**C**) prostate cancer-specific mortality (PCSM) (p=0.00002) for the low and high expression groups of the ten-gene signature (BROMO-10) determined using a median split of the scores in the MCI cohort (n=545)(Erho et al., 2013). The number of patients at risk for each group is show beneath the plot (low and high in the top and bottom raw). The independent prognostic contribution of the BROMO-10 signature over clinicopathological variables as assessed using univariate (**D,F**) and multivariate (**E,G**) analysis and depicted as forest plots applied to the JHMI-RP validation cohort (Ross et al., 2015) for the biochemical recurrence (BCR) endpoint (**D,E**), and in the MCII validation cohort (Karnes et al., 2013) for the prostate cancer-specific mortality (PCSM) endpoint (**F,G**). p-values for each analysis are indicated above the plots. Gleason Score 8 and above with GS 7 as reference (GS8+), lymph node invasion (LNI), surgical margin status (SM) positive, seminal vesicle invasion (SVI), extra capsular extension (ECE), preoperative PSA 10-20 ng/ml

(PSA10TO20), pre-operative PSA 20ng/ml or greater (PSA20+), adjuvant hormone therapy (ADT) and adjuvant radiation therapy (RT) are shown.

Supplemental Experimental Procedures

Clinical material

For Formaldehyde-Assisted Isolation of Regulatory Elements (FAIRE) followed by sequencing (seq) assays and FAIREqPCR assays 40x10µm microtome slides of freshly frozen tissue samples from 3 benign prostate hyperplasia (BPH), 6 primary prostate cancers (PC) and 3 castration resistant prostate cancers (CRPC) were used.
RNA-sequencing data from transcriptomes of 12 BPH, 28 untreated PCs, and 13 CRPCs was retrieved from Ylipaa et al.,(Ylipaa et al., 2015).
DNA methylation data of 3 BPH, 3 primary PCs and 3 CRPCs samples matching RNAseq and FAIRE-seq data were obtained from Kaukoniemi et al. (manuscript in preparation).
For quantitative PCR analysis of mRNA, freshly frozen tissues from 8 BPH and 27 untreated primary PC samples from prostatectomies, as well as 7 BPH and 15 CRPC specimens from transurethral resection of the prostate (TURP) -treated patients were used. The samples were snap frozen in liquid nitrogen and total RNA was isolated with Trizol™-Reagent (Invitrogen Inc., Carlsbad, California, USA) according to manufacturer's instructions. Tumor samples contained, at least, 70% of cancer cells.
The Tampere patients' cohort of tissue microarrays (TMAs) contained a total of 258 formalin-fixed paraffin embedded prostatectomy and 121 CRPC (TURP) specimens obtained from Tampere University Hospital. Subset of the cohort was used to immunostain for ATAD2, BRD2, and BRD4. For the prostatectomy-treated patients, detectable prostate specific antigen (PSA) values (≥0.5 ng/ml) in two consecutive measurements or the emergence of metastases were considered as signs of progression. The use of TMAs and the above mentioned clinical material has been approved by the ethical committee of Tampere University Hospital and the National Authority for Medicolegal Affairs.
The Hamburg patients' TMA cohort contained 9467 prostatectomy tissue specimens. Radical prostatectomy specimens were available from 12,427 patients, undergoing surgery between 1992 and 2012 at the Department of Urology and the Martini Clinics at the University Medical Center Hamburg-Eppendorf. Follow-up data were available for a total of 12,344 patients with a median follow-up of 36 months (range: 1 to 241 months). PSA values were measured following surgery and PSA recurrence was defined as the time point when postoperative PSA was at least 0.2ng/ml and increasing at subsequent measurements. All prostate specimens were analyzed according to a standard procedure, including a complete embedding of the entire prostate for histological analysis(Schlomm et al., 2008). The TMA manufacturing process was described earlier in detail(Kononen et al., 1998). In short, one 0.6mm core was taken from a representative tissue block from each patient. The tissues were distributed among 27 TMA blocks, each containing 144 to 522 tumor samples. For internal controls, each TMA block also contained various control tissues, including normal prostate tissue. The molecular database attached to this TMA contained results on 8q24 FISH analysis (expanded from El Gammal et al., (El Gammal et al., 2010)), Androgen Receptor (AR) expression (expanded from Minner et al.,(Minner et al., 2011)) and Ki67 labeling index (Ki67LI) data (expanded from Minner at al.,(Minner et al., 2010)). Analysis of patient and corresponding histopathological data for research purposes, as well as construction of tissue microarrays from archived diagnostic tissues, was approved by local laws (HmbKHG, §12,1) and by the local ethics committee (Ethics commission Hamburg, WF-049/09 and PV3652).
All work was carried out in compliance with the Helsinki Declaration.

Cell lines and cell culture procedure

Parental LNCaP, VCaP, and 22RV1 cells were purchased from ATCC and maintained according to the manufacturer instructions in RPMI 1640 or DMEM (Gibco, 21875 and 41966) respectively, supplemented with 10% fetal bovine serum (FBS; Gibco, 10500) at 37 °C and 5% CO2. LNCaP-AR model derivative cells overexpressing AR were described previously(Waltering et al., 2009) and were maintained in geneticin 250µg/ml (Gibco, 10131). The hormone treatments were

performed as previously described (Massie et al., 2011; Urbanucci et al., 2008) with minor modifications: the cells were hormone deprived using phenol free RPMI 1640 or DMEM (Gibco, 11835 and 31053). MDV3100 resistant LNCaP were a gift from Professor Donald J. Vander Griend. The cells were first described in Kregel et al. (2013)(Kregel et al., 2013) and maintained in 10uM MDV3100 prior treatment with JQ1 (a kind gift by Professor Stefan Knapp). LNCaP and VCaP cells were hormone starved for three days and subsequently treated with 1 nM R1881 for 4 hours prior being used for other assays. LNCaP-pcDNA3.1, -ARmo and -ARhi cells were hormone-starved for 4 days and subsequently treated with DHT or with equal volume of ethanol vehicle (0 M).

Formaldehyde-Assisted Isolation of Regulatory Elements

Two replicates were processed for each cell line and condition for subsequent sequencing analysis. 3-5 replicates were processed for qPCR analysis. Four million cells were plated and hormone-deprived for 4 days. Cells were then treated with R1881 or DHT as indicated in the text for 4 hours. Cells were fixed by adding formaldehyde (Merck KGaA, Darmstadt, Germany) in 1% final concentration for 10 minutes at room temperature and lysed in 1% SDS, 10 mM EDTA, 50 mM Tris-HCl containing 2X protease inhibitor (Roche Inc., Mannheim, Germany). To perform tissue FAIRE from the clinical material, 3 ml of PBS containing 2X protease inhibitor (Roche Inc., Mannheim, Germany) were added to 40x20 µm sections of freshly frozen tissue specimens. They were first vigorously mixed 3 times with syringe and 14G needle, then 4 times with 25G needle. The cells were fixed for 10 minutes in room temperature by adding 1/10 volume of fixation solution (11% formaldehyde, 0.1 M NaCl, 1 mM EDTA, 0.5 mM EGTA, 50 mM HEPES). Fixation was stopped by adding 1/20 volume of 2.5 M glycine for 5 minutes at room temperature. The cells were pelleted, washed twice in PBS containing 2X protease inhibitor (Roche Inc., Mannheim, Germany) and lysed as above. The chromatin was sonicated to reach a fragment size of 150-300 bp with Bioruptor UCD-200TM-EX instrument (Diagenode Inc., Liège, Belgium).
Three subsequent Phenol:Chloroform:Isoamyl Alcohol (Sigma, P3803) extractions were performed using Phase-Lock heavy tubes (5Prime, 2302830) on the soluble chromatin to isolate protein free DNA in the aqueous phase. The DNA was then further processed as previously described(Urbanucci et al., 2012) prior library preparation with Illumina TrueSeq kit and subsequent sequencing with Illumina HiSeq 2000 or analysed via qPCR.

Chromatin Immunoprecipitation

Chromatin Immunoprecipitation (ChIP) was performed as previously described(Barfeld et al., 2015) using 10 µg of normal rabbit IgG (Santa Cruz Inc., Santa Cruz, California, USA) or 10 µl of N20 AR antibody (Santa Cruz Inc., Santa Cruz, California, USA) previously incubated o/n with magnetic Diagenode beads. The DNA was then purified as previously described(Urbanucci et al., 2012).

RNA isolation and processing for microarrays

Total RNA was isolated using the Qiagen RNeasy kit (Qiagen, 74106) following the manufacturer's recommendations. RNA concentration and purity was measured using a NanoDrop instrument (Thermo Scientific).

Quantitative PCR

For mRNA expression analyses from cell-lines, 500ng to 1µg total RNA were reverse transcribed using the SuperScript VILO kit (Applied Biosystems, 11754) following the manufacturer's recommendations. qRT-PCR was performed using SYBR green master mix (Applied Biosystems, 4385612). Amplification was performed in duplicate series using the ABI 7900HT. The relative expression of each gene against the average value of *TBP* or *β-actin* reference genes was measured using SYBR green master mix (Applied Biosystems, 4385612) and then normalized to vehicle

condition. qRT-PCR of clinical material was performed as previously described(Urbanucci et al., 2012).
For the ChIP-qPCR or FAIRE-qPCR analysis, the enrichment relative to input chromatin was calculated according to the delta Ct method with the percentages being calculated using the formula $2^{-\Delta Ct}$, where ΔCt is Ct(ChIP-template)-Ct(Input), essentially as previously described(Urbanucci et al., 2012). The primers used are listed below (NB. Marked regions refer to **Data Supplemental File 1**):-

FAIREqPCR	
PSA enhancer fw	TGGGACAACTTGCAAACCTG
PSA enhancer rev	CCAGAGTAGGTCTGTTTTCAATCCA
PSA mid region fw	CAGTGGCCATGAGTTTTGTTTG
PSA mid region rev	AACCAATCCAACTGCATTATACACA
PSA promoter fw	CCTAGATGAAGTCTCCATGAGCTACA
PSA promoter rev	GGGAGGGAGAGCTAGCACTTG
H3K27me3-marked region 1 fw	AGAAGCTAAATTAGATACAA
H3K27me3-marked region 1 rev	AGTAAATTTTTCATTCATAC
H3K27me3-marked region 2 fw	TGTTCACCAAATACTGGAGA
H3K27me3-marked region 2 rev	AGTGGGTTTTTGAAGTCTCT
TMPRSS2 promoter fw	GCTCGAGTTTGGGTTAAGGAA
TMPRSS2 promoter rev	TACAGGAGCTCGTGAGGTAGCA
TMPRSS2 enhancer fw	TCCAGGCAGAGGTGTGGC
TMPRSS2 enhancer rev	CGTATGTCTCCCTGCACCACT
UBE2C fw	CACGCGGAGTAAGACGTGTA
UBE2C rev	CGTTGGAAAACGCTAACCAT
HOXB13_TSS fw	AACCATGACCTGCTTTGGTC
HOXB13_TSS rev	TGCCTGGGTAATTCACCATT
HOXB13_ARBS fw	TCCCCTTTCTCAGATGGATG
HOXB13_ARBS rev	TTTCACCACCCTGCTTTCTC
AURKA_TSS fw	CTCGTCCGCCACTGAGATA
AURKA_TSS rev	TTGGAAGACTTGGGTCCTTG
AURKA_ARBS fw	TTTGCAGCCCTAGAGCAAAT
AURKA_ARBS rev	TCAGACAATGACACATTCATGC
CAMKK2_ARBS fw	AGAACACTGTAGCTCACACAGGCA
CAMKK2_ARBS rev	GGGCACTTCCCAACCTTTCTTACT
ChIPqPCR	
BRD4_prox fw	ATCTCCAGCCGTCTGTTTGT
BRD4_prox rev	GAGTGAGCTCAGCCTCCTTG
BRD4_far fw	CTTTTGGCATGGCTCAGAGT
BRD4_far rev	TGTGGCAGGAAATGAACAAG
BRD2 fw	TGTGCTTGTTTGCCTTTCTG
BRD2 rev	TGGCTCAGTTCCAGTTGCTT

ATAD2 fw	TGTTCAGCAACATCATAGTCCA
ATAD2 rev	GGAAACAAATGTTCAGCAAGAA
RT-PCR	
BRD4-L fw	CTGGACCAGCAGAGGGAGT
BRD4-L rev	ACCTAGGTGCGCTCAGAAAA
BRD4-S fw	GACAGCGAAGACTCCGAAAC
BRD4-S rev	TGGGAAGGAATCTGGAACTG
BRD2 fw	TGAAACACTCAAGCCATCCA
BRD2rev	CCTCCTTTGTCTTTCCCACA
ATAD2 fw	CATCGCAAGGACCATGATAA
ATAD2 rev	TCAATTAGGCGGACATGACA
PSA fw	GCAGCATTGAACCAGAGGAG
PSA rev	AGAACTGGGGAGGCTTGAGT
TMPRSS2 fw	CCAGGAGTGTACGGGAATGT
TMPRSS2 rev	CAGCCCCATTGTTTTCTTGT
CAMKK2 fw	TGAAGACCAGGCCCGTTTCTACTT
CAMKK2 rev	TGGAAGGTTTGATGTCACGGTGGA
HOXB13 fw	AGATGTGTTGCCAGGGAGAA
HOXB13 rev	CTTGCTGTACGGAATGCGTT
AURKA fw	AGGCCACTGAATAACACCCA
AURKA rev	TGATGCCAGTTCCTCCTCAG
UBE2C fw	TGGCGATAAAGGGATTTCTGC
UBE2C rev	CGCATTGTAAGGGTAGCCAC
HIST2H4B fw	CTCAGGCAAAGTGGGAGAAG
HIST2H4B rev	AAGCCCAAAACAGTCAATCG
H1H3H fw	CAGAAAGCTGCCTTTTCAGC
H1H3H rev	GGTTGGTGTCCTCAAAGAGC
H2H2BE fw	TCAGAGCCACCCACCTAATC
H2H2BE rev	GTATGCCATTTCCCATGACC
HIST1H2AC fw	CTCCGTAAAGGCAACTACGC
HIST1H2AC rev	TGCGAGTCTTCTTGTTGTCG
HIST2H2AA3 fw	AATAGCGAACCTGGAGCTGA
HIST2H2AA3 rev	GAAGAGCCAAGGCAGTTACG
TBP fw	GGGGAGCTGTGATGTGAAGT
TBP rev	GAGCCATTACGTCGTCTTCC
B-Actin	TGGGACGACATGGAGAAAAT
B-Actin	AGAGGCGTACAGGGATAGCA
G3PDH2 fw	TGAGGAGGGGAGATTCAGTG
G3PDH2 rev	GTCAGTGGTGGACCTGACCT

Transcript expression profiling (mRNA)
For microarray analysis, RNA integrity was confirmed using a 2100 Bioanalyzer (Agilent) and Total RNA Nano Chip (Agilent, 5067-1511). 500ng RNA were reverse transcribed and Biotin-labeled using the TotalPrep-96 RNA Amplification kit (Illumina, 4393543) following the manufacturer's recommendations. Resuspended cRNA samples were hybridized onto Human HT-12 Expression BeadChips (Illumina, BD-103-0204). Missing probes were imputed using Illumina's GenomeStudio Gene Expression Module.
Analysis of microarray data from JQ1/R1881 treated cells was performed as follows: the imputed probe datasets were analyzed using the freely available J-Express 2012 software (http://jexpress.bioinfo.no/site/). The raw data was quantile normalized and log2 transformed prior to analysis. Differential expression analysis was performed using the grouped triplicate experiments and Rank product analysis. Probes with a q-value of <0.05 were considered significantly up- or downregulated. The data are deposited in GEO: GSE73989.

ChIP/DHS-seq re-analysis and FAIRE-seq analysis
ChIP-seq data for AR and ERG were retrieved from (Massie et al., 2011; Sharma et al., 2013; Yu et al., 2010)
The raw reads from described studies were mapped with novoalign (http://www.novocraft.com) and to the human reference genome (build hg19) with default parameters. A maximum of 5 read duplicates per genomic location was allowed by our filtering. Peak detection (i.e., binding site detection) of the chromatin immunoprecipitation (ChIP) and DNA hypersensitive sites (DHS) –seq was performed as previously described(Urbanucci et al., 2012).
Peak detection for FAIRE-seq was performed using MACS(Zhang et al., 2008) with default parameters using inputs of each of the FAIRE samples as controls, and with F-Seq(Boyle et al., 2008). F-seq was used taking into account genomic mappability background and copy number/karyotype correction. The human genome background files were downloaded directly from F-seq website resource (http://fureylab.web.unc.edu/software/fseq/). To correct for copy number/karyotype for our cell lines, we created iff files using iffBuilder (http://fureylab.web.unc.edu/software/fseq/). iffBuilder was fed with chromosome-wise wiggle files produced from the input of each FAIRE sample. To produce wiggle files we used a python based script "create_depth_track_window.py" using a 1000bp sliding window at a step=1. See below:-

Python script used to generate wig files to feed IffBuilder, Related to Experimental Procedure

```
#!usr/bin/env python

import sys, string

if (len(sys.argv) == 1):
  print "Run as:\n"
  print "python create_depth_track_window.py ifolder ifile ofolder win_size [-zig] [-hg18]\n"
  print "- ifolder:  folder containing the input file"
  print "- ifile:    the input file (a coordinate-sorted bed file)"
  print "- ofolder:  folder for output files"
  print "- win_size: size of the sliding window"
  print "- [-zig]  : optional parameter, if \"-zig\" is present as an argument, bases with zero coverage will
be ignored during the computation of mean genomic sequencing depth"
  print "- [-hg18]:  optional parameter, if \"-hg18\" is present as an argument, the script works with
chromosome sizes derived from human genomic build hg18\n"
  sys.exit(0)

# input folder - folder containing the input file
ifolder = sys.argv[1]

if (ifolder[-1:] != "/"):
  ifolder = ifolder + "/"
```

```
# input file - a coordinate-sorted bed file
ifile = open(ifolder + sys.argv[2], "r")

# output folder - folder in which the output files should be stored
ofolder = sys.argv[3]

if (ofolder[-1:] != "/"):
   ofolder = ofolder + "/"

# sliding window size
win_size = int(sys.argv[4])

chrom_sizes =

# hg19 chromosome sizes
chrom_sizes["chr1"] = 249250621
chrom_sizes["chr2"] = 243199373
chrom_sizes["chr3"] = 198022430
chrom_sizes["chr4"] = 191154276
chrom_sizes["chr5"] = 180915260
chrom_sizes["chr6"] = 171115067
chrom_sizes["chr7"] = 159138663
chrom_sizes["chr8"] = 146364022
chrom_sizes["chr9"] = 141213431
chrom_sizes["chr10"] = 135534747
chrom_sizes["chr11"] = 135006516
chrom_sizes["chr12"] = 133851895
chrom_sizes["chr13"] = 115169878
chrom_sizes["chr14"] = 107349540
chrom_sizes["chr15"] = 102531392
chrom_sizes["chr16"] = 90354753
chrom_sizes["chr17"] = 81195210
chrom_sizes["chr18"] = 78077248
chrom_sizes["chr19"] = 59128983
chrom_sizes["chr20"] = 63025520
chrom_sizes["chr21"] = 48129895
chrom_sizes["chr22"] = 51304566
chrom_sizes["chrX"] = 155270560
chrom_sizes["chrY"] = 59373566
chrom_sizes["chrM"] = 16571

if ("-hg18" in sys.argv):
   chrom_sizes["chr1"] = 247249719
   chrom_sizes["chr2"] = 242951149
   chrom_sizes["chr3"] = 199501827
   chrom_sizes["chr4"] = 191273063
   chrom_sizes["chr5"] = 180857866
   chrom_sizes["chr6"] = 170899992
   chrom_sizes["chr7"] = 158821424
   chrom_sizes["chr8"] = 146274826
   chrom_sizes["chr9"] = 140273252
   chrom_sizes["chr10"] = 135374737
   chrom_sizes["chr11"] = 134452384
   chrom_sizes["chr12"] = 132349534
   chrom_sizes["chr13"] = 114142980
   chrom_sizes["chr14"] = 106368585
   chrom_sizes["chr15"] = 100338915
   chrom_sizes["chr16"] = 88827254
   chrom_sizes["chr17"] = 78774742
   chrom_sizes["chr18"] = 76117153
   chrom_sizes["chr19"] = 63811651
```

```
   chrom_sizes["chr20"] = 62435964
   chrom_sizes["chr21"] = 46944323
   chrom_sizes["chr22"] = 49691432
   chrom_sizes["chrX"] = 154913754
   chrom_sizes["chrY"] = 57772954
   chrom_sizes["chrM"] = 16571

   print "Optional parameter \"-hg18\" recognized: the script will be working with chromosome sizes
derived from human genomic build hg18.\n"
else:
   print "Optional parameter \"-hg18\" not recognized: the script will be working with chromosome sizes
derived from human genomic build hg19.\n"
pos_vals = {}   # relevant positions on currently processed chromosome and their seq. depth
final_pos_vals = {}   # values for positions that can no longer be updated (ready for ouput if all values in
given sliding window are available)
out_FPV = 0   # last output position (passed from final_pos_vals to the output)
out_sum_FPV = 0   # sum of sequencing depths for all bases inside the sliding window
elem_count_FPV = 0   # number of bases inside the sliding window
max_FPV = 0   # current maximum position in the final_pos_vals directory

val_distrib = {}   # abundances of sequencing depth values

last_chrom = ""   # chromosome of the last processed read
last_pos = 0   # last genomic position passed from pos_vals to final_pos_vals

# an output buffer and its maximal allowed size
out_buffer = ""
out_buffer_size = 0
out_buffer_max_size = 1024*1024*16

ofile = ""

zero_pos = 0
non_zero_pos = 0
cov_sum = 0

for line in ifile:
   line = string.strip(line)
   line_s = line.split()

   chrom = line_s[0]
   s_pos = int(line_s[1]) + 1
   e_pos = int(line_s[2])

   # upon chromosome change:
   # empty pos_vals and process any trailing zero-depth positions, change the output file
   if not (chrom == last_chrom):

      if not (last_chrom == ""):

         if (len(out_buffer) > 0):
            ofile.write(out_buffer)
            out_buffer = ""
            out_buffer_size = 0

         for i in range(last_pos + 1, chrom_sizes[last_chrom] + 1):

            if (pos_vals.has_key(i)):
               final_pos_vals[i] = pos_vals[i]
               max_FPV = i

               if not (val_distrib.has_key(pos_vals[i])):
```

```
            val_distrib[pos_vals[i]] = 1
          else:
            val_distrib[pos_vals[i]] += 1

          non_zero_pos += 1
          cov_sum += pos_vals[i]
          del(pos_vals[i])

        else:
          max_FPV = i

          if not (val_distrib.has_key(0)):
            val_distrib[0] = 1
          else:
            val_distrib[0] += 1

          zero_pos += 1

      for i in range(out_FPV + 1, chrom_sizes[last_chrom] + 1):

        if (i == 1):
          for j in range(1, win_size/2 + 1):
            elem_count_FPV += 1
            if (final_pos_vals.has_key(j)):
              out_sum_FPV += final_pos_vals[j]

        if (i - win_size/2 > 1):
          elem_count_FPV -= 1

          if (final_pos_vals.has_key(i - win_size/2 - 1)):
            out_sum_FPV -= final_pos_vals[i - win_size/2 - 1]
            del(final_pos_vals[i - win_size/2 - 1])

        if (i + win_size/2 <= chrom_sizes[last_chrom]):
          elem_count_FPV += 1

          if (final_pos_vals.has_key(i + win_size/2)):
            out_sum_FPV += final_pos_vals[i + win_size/2]

        outval = round(float(out_sum_FPV)/elem_count_FPV, 4)
        ofile.write(str(outval) + "\n")

      final_pos_vals = {}
      out_FPV = 0
      out_sum_FPV = 0
      elem_count_FPV = 0
      max_FPV = 0

      pos_vals = {}
      last_pos = 0

    if not (ofile == ""):
      ofile.close()
    ofile = open(ofolder + sys.argv[2] + "." + chrom, "w")
    print("Creating a smooth coverage profile for chromosome " + chrom + " ..\n")
    last_chrom = chrom

  # output values for genommic positions that can't get updated anymore
  if (s_pos > last_pos + 1):
    for i in range(last_pos + 1, s_pos):
      if (pos_vals.has_key(i)):
        final_pos_vals[i] = pos_vals[i]
```

```
        max_FPV = i

        if not (val_distrib.has_key(pos_vals[i])):
          val_distrib[pos_vals[i]] = 1
        else:
          val_distrib[pos_vals[i]] += 1

        non_zero_pos += 1
        cov_sum += pos_vals[i]

        del(pos_vals[i])

      else:
        max_FPV = i

        if not (val_distrib.has_key(0)):
          val_distrib[0] = 1
        else:
          val_distrib[0] += 1

        zero_pos += 1

    last_pos = s_pos - 1

    if (out_FPV + 1 + win_size/2 <= max_FPV):
      for i in range(out_FPV + 1, max_FPV - win_size/2 + 1):

        if (i == 1):
          for j in range(1, win_size/2 + 1):
            elem_count_FPV += 1
            if (final_pos_vals.has_key(j)):
              out_sum_FPV += final_pos_vals[j]

        if (i - win_size/2 > 1):
          elem_count_FPV -= 1

          if (final_pos_vals.has_key(i - win_size/2 - 1)):
            out_sum_FPV -= final_pos_vals[i - win_size/2 - 1]
            del(final_pos_vals[i - win_size/2 - 1])

        if (i + win_size/2 <= chrom_sizes[last_chrom]):
          elem_count_FPV += 1

          if (final_pos_vals.has_key(i + win_size/2)):
            out_sum_FPV += final_pos_vals[i + win_size/2]

        outval = round(float(out_sum_FPV)/elem_count_FPV, 4)
        out_buffer += str(outval) + "\n"
        out_buffer_size += 1

        if (out_buffer_size > out_buffer_max_size):
          ofile.write(out_buffer)
          out_buffer = ""
          out_buffer_size = 0

      out_FPV = max_FPV - win_size/2

  # update the pos_vals dictionary (increment for genomic positions s_pos to e_pos)
  for i in range(s_pos, e_pos + 1):
    if not (pos_vals.has_key(i)):
      pos_vals[i] = 1
    else:
```

```
        pos_vals[i] += 1

ifile.close()

# empty pos_vals and process trailing zero-depth positions for the last chromosome
if (len(out_buffer) > 0):
   ofile.write(out_buffer)
   out_buffer = ""
   out_buffer_size = 0

for i in range(last_pos + 1, chrom_sizes[last_chrom] + 1):
   if (pos_vals.has_key(i)):
      final_pos_vals[i] = pos_vals[i]
      max_FPV = i

      if not (val_distrib.has_key(pos_vals[i])):
         val_distrib[pos_vals[i]] = 1
      else:
         val_distrib[pos_vals[i]] += 1

      non_zero_pos += 1
      cov_sum += pos_vals[i]

      del(pos_vals[i])

   else:
      max_FPV = i

      if not (val_distrib.has_key(0)):
         val_distrib[0] = 1
      else:
         val_distrib[0] += 1

      zero_pos += 1

for i in range(out_FPV + 1, chrom_sizes[last_chrom] + 1):

   if (i == 1):
      for j in range(1, win_size/2 + 1):
         elem_count_FPV += 1
         if (final_pos_vals.has_key(j)):
            out_sum_FPV += final_pos_vals[j]

   if (i - win_size/2 > 1):
      elem_count_FPV -= 1

      if (final_pos_vals.has_key(i - win_size/2 - 1)):
         out_sum_FPV -= final_pos_vals[i - win_size/2 - 1]
         del(final_pos_vals[i - win_size/2 - 1])

   if (i + win_size/2 <= chrom_sizes[last_chrom]):
      elem_count_FPV += 1

      if (final_pos_vals.has_key(i + win_size/2)):
         out_sum_FPV += final_pos_vals[i + win_size/2]

   outval = round(float(out_sum_FPV)/elem_count_FPV, 4)
   ofile.write(str(outval) + "\n")

final_pos_vals = {}
out_FPV = 0
out_sum_FPV = 0
```

```
elem_count_FPV = 0
max_FPV = 0

last_pos = 0

ofile.close()

# output the depth distribution values
dist_values = val_distrib.keys()
dist_values.sort()

genome_length = 0

for chrom in chrom_sizes:
   genome_length += chrom_sizes[chrom]

dfile = open(ofolder + sys.argv[2] + ".depth_value_distribution", "w")
dfile.write("# assembly: hg19\n")
dfile.write("# total genome length: " + str(genome_length) + " bp\n")
dfile.write("# column seq_depth: sequencing depth\n")
dfile.write("# column bp_count: number of genomic locations (1-bp sites) with respective sequencing
depth\n")
dfile.write("# column genome_fraction_%: column bp_count expressed as fraction of the genome
length\n")
dfile.write("# column acc_genome_fraction_%: accumulation of values from column
genome_fraction_%\n")
dfile.write("seq_depth\tbp_count\tgenome_fraction_%\tacc_genome_fraction_%\n")

acc_b_count = 0

for value in dist_values:
   b_count = val_distrib[value]
   acc_b_count += b_count
   g_fraction = round(float(b_count)*100/genome_length, 5)
   acc_g_fraction = round(float(acc_b_count)*100/genome_length, 5)

   dfile.write(str(value) + "\t" + str(b_count) + "\t" + str(g_fraction) + "\t" + str(acc_g_fraction) + "\n")

dfile.close()

print("Number of zero-coverage positions: " + str(zero_pos))
print("Number of non-zero-coverage positions: " + str(non_zero_pos))
print("Total number of genomic positions: " + str(zero_pos + non_zero_pos) + " (check: " +
str(genome_length) + ")")
print("Total coverage sum: " + str(cov_sum))
print("Genomic mean (zero-coverage positions considered): " +
str(round(float(cov_sum)/(zero_pos+non_zero_pos), 4)))
print("Genomic mean (zero-coverage positions not considered): " +
str(round(float(cov_sum)/non_zero_pos, 4)) + "\n")

gen_mean = float(cov_sum)/(zero_pos+non_zero_pos)

if ("-zig" in sys.argv):
   gen_mean = float(cov_sum)/non_zero_pos
   print "Optional parameter \"-zig\" recognized: bases with zero coverage are not considered in the
genomic mean computation.\n"
else:
   print "Optional parameter \"-zig\" not recognized: bases with zero coverage are considered in the
genomic mean computation.\n"

for chrom_name in chrom_sizes:
   print("Creating a wiggle file for chromosome " + chrom_name + " ..\n")
```

```
    cdfile = open(ofolder + sys.argv[2] + "." + chrom_name, "r")
    wigfile = open(ofolder + sys.argv[2] + "." + chrom_name + ".wig", "w")

    out = False
    start_offset = 1

    for inline in cdfile:

      inline = string.strip(inline)

      if ((not out) and (float(inline) == 0.0)):
        start_offset += 1

      elif ((not out) and (float(inline) != 0.0)):
        out = True
        wigfile.write("fixedStep chrom=" + chrom_name + " start=" + str(start_offset) + " step=1\n")
        wigfile.write(str(round(float(inline)/gen_mean, 4)) + "\n")

      else:
        wigfile.write(str(round(float(inline)/gen_mean, 4)) + "\n")

    cdfile.close()
    wigfile.close()

print "All done.\n"
```

FAIRE-seq analysis (continued)

F-Seq was run twice, overlapping peaks from both iterations were then overlapped with MACS peaks. As we had run two biological replicates of the FAIRE samples, we further overlapped the resulting intervals of the corresponding replicates.

For FAIRE-seq from the clinical samples FSeq iteration was repeated twice and resulting bed files were intersected as indicated in the text (category-wise or disease-stage wise) in order to produce consensus open chromatin regions.

The data are deposited in GEO: GSE73989.

Chromatin shape was assessed via FAIRE-seq normalized read counts within the FAIRE-seq peaks indicating chromatin open regions. This is a measure of the potency of the opening events within 1 Kb upstream annotated genes.

Gene-wise correlation between gene expression and local chromatin accessibility or local DNA methylation in prostate benign and cancer tissues samples (Figure 1)

Gaussian distribution deviation from a random distribution of correlative events between raw sequencing reads included within FAIRE-seq peaks or DNA methylated regions and transcript levels (measured as average reads counts) of gene transcription start sites (TSSs) were calculate across a number of intervals. This analysis was supported by the Kolmogorov-Smirnov statistic test shown in **Figure 1E-F**, in the main text. The test verified the statistical significance of the shift of the correlative events (in blue) from the random distribution (in red). A small shift of the Gaussian distributed curve toward the right indicated a correlation of local (as indicated by the intervals) open chromatin and increased gene expression. On the contrary, a small shift to the left indicated a correlation of local (as indicated by the intervals) DNA methylation with low gene expression. When correlation between gene expression and open chromatin upstream the TSS was considered, the Kolmogorov-Smirnov statistic test showed a marked deviation from the random correlation events. Up to a distance of 250kb upstream the TSS, this deviation grows and indicated an increased probability of encountering regulatory regions bound by transcription factors, before decreasing again 500 kb or 1Mb upstream the TSSs (**Figure 1F**). When, on the contrary, correlation between gene expression and local open chromatin around the TSS is considered, the Kolmogorov-Smirnov statistic test showed an indiscriminate deviation from the random correlation events (**Figure 1F**),

indicating the presence of confounding factors such as gene bodies or downstream genes that are actively transcribed. For genomic intervals bigger than 250kb, the shift returned, which once again, indicated the presence of confounding factors such as the presence of other genes (**Figure 1G**).

Reads distribution around peaks, motif enrichment, peaks distribution analysis, gene set enrichment analysis and gene ontology

Read distribution analysis around centre feature peaks was performed using a script(Hurtado et al., 2011) which generate a matrix of " normalized differences between coverage integrals in treated (e.g. FAIRE) versus control (e.g. Input) samples aligned reads" around a certain base pairs window (eg 5 kb). The normalization depends only on the dataset sizes computed as 10M/dataset_size. The script was modified to inspect reads distribution around windows larger than 5 kb.

To assess the presence of motifs of transcription factors (TFs) in the FAIRE-seq dataset, we looked for overrepresented TF motifs in open regions. Prediction of TF binding was performed using "findMotifsGenome.pl", and peaks distribution analysis with annotatePeaks.pl, both parts of the HOMER package(Heinz et al., 2010). Gene set enrichment analysis (GSEA) was performed by applying GSEA v2.07 (Broad Institute(Subramanian et al., 2005)) on a publicly available dataset of 150 AR target genes in castration resistant prostate cancer derived from Sharma et al.,(Sharma et al., 2013). This dataset was tested for enrichment in gene expression data from LNCaP and VcaP cells cultured in presence of JQ1. Gene ontology (GO) of up and down regulated genes upon treatment of the same cells was performed using GOrilla(Eden et al., 2009).

Evaluation of the 15-gene signature prognostic value

Microarray data from the Decipher GRID™ were extracted for three radical prostatectomy cohorts from previously described(Erho et al., 2013; Karnes et al., 2013; Ross et al., 2015) validation studies. Specimen selection, RNA extraction and microarray hybridization was performed for these samples in a Clinical Laboratory Improvement Amendments (CLIA)-certified laboratory facility (GenomeDx Biosciences, San Diego, CA, USA) as previously described(Erho et al., 2013; Ross et al., 2015). Briefly, total RNA was extracted and purified using the Ovation WTA FFPE system (NuGen, San Carlos, CA). RNA was amplified and labeled using the Ovation WTA FFPE system (NuGen, San Carlos, CA) and hybridized to Human Exon 1.0 ST GeneChips (Affymetrix, Santa Clara, CA). After microarray quality control using the Affymetrix Power Toosl packages, probeset normalization was performed using the Single Channel Array Normalization (SCAN) algorithm(Piccolo et al., 2012). Affymetrix Core level summaries for annotated genes were used to summarize gene expression.

A classifier to distinguish between metastatic vs. non-metastatic cancers was developed. Metastatic progression after prostatectomy was defined as a positive CT scan or bone scan. The prognostic value of the signature was further assessed for biochemical recurrence and death from prostate cancer. The classifier was constructed using a generalized linear model with elastic net regularization as previously described(Erho et al., 2013).

Statistical analyses were performed in R, version 3.2.2, all statistical tests were two-sided using a 5% significance level, and the model was constructed using the glmenet package (glmnet_2.0-2). The value of lambda was determined using a 10-fold cross-validation in glmnet. The model was generated using the MCI cohort (GSE46691) as training data. In the final model 10 of the 15 genes contributed to the model score with 6 positively associated and 4 negatively associated genes as determined by the regularized coefficients. The final model output a continuous variable score ranging between 0 and 1 with higher scores indicating a higher probability of metastasis. Scores were then generated for samples from the Mayo Clinic II (MCII) and JHMI-RP validation cohorts and performance in each cohort was assessed using survival analysis. Kaplan-Meier curve p-values were generated with a weighted Cox regression model (R package survival_2.38-3).

Univariableand multivarible Cox proportional hazards analyses were performed using the cch method implemented in the survival package

Immunohistochemistry
In the Tampere TMA cohort, mouse anti-ATAD2 (HPA029424), anti-BRD2 (Bethyl Laboratories, Inc., Montgomery, TX, USA), and anti-BRD4 (Bethyl Laboratories, Inc., Montgomery, TX, USA) were used with Power Vision+ Poly-HRP IHC kit (ImmunoVision Technologies Co., Burlingame, California, USA) according to the manufacturer's instructions. The protocol has previously been described(Leinonen et al., 2010).
BRD2 and BRD4 were scored like in the human protein atlas project: the intensity of staining was scored semiquantitatively (0-3) plus the area percentage (0%, <25%, 25-75%, >75%). Both cytoplasmic and nuclear staining for ATAD2 were scored for intensity (0-3) and percentage (0-100). No digital imagae analysis was used.
The anti-ATAD2 antibody was also used for the Hamburg TMA cohort.
Freshly cut TMA sections were immunostained on one day and in one experiment. Slides were deparaffinized and exposed to heat-induced antigen retrieval for 5 minutes in an autoclave at 121°C in pH 7.8 Tris-EDTA-Citrate buffer. Primary antibody specific for ATAD2 (rabbit polyclonal antibody, Sigma, St. Louis, MO, USA; HPA029424; dilution 1:450) was applied at 37°C for 60 minutes. Bound antibody was then visualized using the EnVision Kit (Dako, Glostrup, Denmark) according to the manufacturer´s directions. Only nuclear ATAD2 staining was evaluated.

siRNA transfections
Silencer® selected siRNAs from Ambion (Applied biosystems/Ambion, Austin, Texas, USA) were used. Cells were reverse-transfected with lipofectamin RNAiMAX transfection reagent (Invitrogen, 13788) according to the manufacturer's protocol. Briefly, the cells were seeded and transfected with 20 nM of siBRD2 (s12070), 20 nM of siBRD4 (s23903), 20 nM of siATAD2 (s26393) or equal concentration of *Silencer*® negative control siRNA #1. Expression levels of *BRD2*, *BRD4* and *ATAD2* relative to *TBP* were measured by qRT-PCR (2.5 days after transfection) and protein levels by Western blot analysis (3 days after transfection).

Viability assays
Viability upon treatment of drugs or gene silencing was assessed using CellTiter-Glo reagent (G3581, Promega, Stockholm, Sweden) MTS assay according to manufacturer's instructions. Colorimetric changes were assessed using a PerkinElmer EnVision® Multilabel Plate Reader.

Fluorescent-based caspase cleavage assay
Appropriate amounts of LNCaP or VCaP cells were seeded in 384-well plates and allowed to attach for 48h at which point they received drug treatment (12 wells per condition). Induction of apoptosis was monitored using the CellPlayer 96-well Caspase-3/7 reagent (Essen Bioscience, 4440) at a final concentration of 1:5,000 on the Incucyte FLR instrument (Essen Bioscience). Phase contrast and fluorescence pictures were taken every two hours for a total of 96h. Analysis was performed using the inbuilt object counting algorithm.

Western Blot analysis
Cells were trypsinized and washed with cold PBS prior to resuspension in RIPA lysis buffer (30 mM Tris-HCl, 150 mM NaCl, 1 mM EDTA, 0.5 % NP40, 0.1 % Na-Deoxycholate, 0.1 % SDS, pH 7.4) supplemented with protease inhibitors (Roche, 11873580001), rotated at 4 °C for 10 min and sonicated in a Bioruptor NextGen (Diagenode) at maximum power for ten cycles of 30 s ON, 30 s OFF to break nuclei and other cellular structures. Lysates were centrifuged for 10 min at 18,000 g and 4 °C and the supernatant transferred to a new tube. Protein concentration was determined using a BCA assay (Pierce, 23227) and equalized with RIPA buffer. Extracts were mixed with LDS NuPAGE buffer (Life technologies, NP0008) and Sample Reducing Agent (Life technologies, NP0009) and denatured for 10 min at 70 °C. Equal amounts were loaded onto 4-12 % gradient Bis-Tris NuPAGE gels (Life technologies, NP0323). Separated proteins were wet-blotted (25 mM Tris-Base, 192 mM glycine, 20 % methanol, 0.01 % SDS, pH 9.2) to methanol-activated 0.45 um PVDF

membranes (Millipore, IPVH00010) for 60 min at 30 V. Membranes were blocked in 5 % BSA (Sigma, A2153) in TBS with 0.1 % Tween-20 (Sigma, P5927) for 1 h prior to overnight incubation with appropriate concentrations of primary antibodies. The next day, membranes were washed with TBS with 0.1 % Tween-20 and incubated with appropriate secondary antibody for 1 h at room temperature. After washing with TBS with 0.1 % Tween-20, membranes were developed using the Novex ECL Reagent kit (Life technologies, WP20005) or a super-sensitive HRP substrate (Rockland, FEMTOMAX-110). Primary antibodies used were ATAD2 (Sigma, HPA029424), BRD2 (abcam, ab139690), MYC (Abcam, ab32072), BRD4 (Sigma, AV39076), KLK3 (Dako, D0487), AR (N-20 sc-816), b-actin-HRP (Cell Signaling, 5125) and GAPDH (Cell Signaling, 2118). Secondary HRP-conjugated anti-rabbit and anti-mouse were purchased from Dako (P0448 and P0447, respectively).

Supplemental References

Barfeld, S.J., Fazli, L., Persson, M., Marjavaara, L., Urbanucci, A., Kaukoniemi, K.M., Rennie, P.S., Ceder, Y., Chabes, A., Visakorpi, T., *et al.* (2015). Myc-dependent purine biosynthesis affects nucleolar stress and therapy response in prostate cancer. Oncotarget *6*, 12587-12602.

Boyle, A.P., Guinney, J., Crawford, G.E., and Furey, T.S. (2008). F-Seq: a feature density estimator for high-throughput sequence tags. Bioinformatics *24*, 2537-2538.

Eden, E., Navon, R., Steinfeld, I., Lipson, D., and Yakhini, Z. (2009). GOrilla: a tool for discovery and visualization of enriched GO terms in ranked gene lists. BMC bioinformatics *10*, 48.

El Gammal, A.T., Bruchmann, M., Zustin, J., Isbarn, H., Hellwinkel, O.J., Kollermann, J., Sauter, G., Simon, R., Wilczak, W., Schwarz, J., *et al.* (2010). Chromosome 8p deletions and 8q gains are associated with tumor progression and poor prognosis in prostate cancer. Clin Cancer Res *16*, 56-64.

Erho, N., Crisan, A., Vergara, I.A., Mitra, A.P., Ghadessi, M., Buerki, C., Bergstralh, E.J., Kollmeyer, T., Fink, S., Haddad, Z., *et al.* (2013). Discovery and validation of a prostate cancer genomic classifier that predicts early metastasis following radical prostatectomy. PloS one *8*, e66855.

Heinz, S., Benner, C., Spann, N., Bertolino, E., Lin, Y.C., Laslo, P., Cheng, J.X., Murre, C., Singh, H., and Glass, C.K. (2010). Simple Combinations of Lineage-Determining Transcription Factors Prime cis-Regulatory Elements Required for Macrophage and B Cell Identities. Molecular cell *38*, 576-589.

Hurtado, A., Holmes, K.A., Ross-Innes, C.S., Schmidt, D., and Carroll, J.S. (2011). FOXA1 is a key determinant of estrogen receptor function and endocrine response. Nat Genet *43*, 27-33.

Karnes, R.J., Bergstralh, E.J., Davicioni, E., Ghadessi, M., Buerki, C., Mitra, A.P., Crisan, A., Erho, N., Vergara, I.A., Lam, L.L., *et al.* (2013). Validation of a genomic classifier that predicts metastasis following radical prostatectomy in an at risk patient population. The Journal of urology *190*, 2047-2053.

Kononen, J., Bubendorf, L., Kallioniemi, A., Barlund, M., Schraml, P., Leighton, S., Torhorst, J., Mihatsch, M.J., Sauter, G., and Kallioniemi, O.P. (1998). Tissue microarrays for high-throughput molecular profiling of tumor specimens. Nature medicine *4*, 844-847.

Kregel, S., Kiriluk, K.J., Rosen, A.M., Cai, Y., Reyes, E.E., Otto, K.B., Tom, W., Paner, G.P., Szmulewitz, R.Z., and Vander Griend, D.J. (2013). Sox2 Is an Androgen Receptor-Repressed Gene That Promotes Castration-Resistant Prostate Cancer. PloS one *8*, e53701.

Leinonen, K.A., Tolonen, T.T., Bracken, H., Stenman, U.H., Tammela, T.L., Saramaki, O.R., and Visakorpi, T. (2010). Association of SPINK1 expression and TMPRSS2:ERG fusion with prognosis in endocrine-treated prostate cancer. Clin Cancer Res *16*, 2845-2851.

Massie, C.E., Lynch, A., Ramos-Montoya, A., Boren, J., Stark, R., Fazli, L., Warren, A., Scott, H., Madhu, B., Sharma, N., *et al.* (2011). The androgen receptor fuels prostate cancer by regulating central metabolism and biosynthesis. EMBO J *30*, 2719-2733.

Minner, S., Enodien, M., Sirma, H., Luebke, A.M., Krohn, A., Mayer, P.S., Simon, R., Tennstedt, P., Muller, J., Scholz, L., *et al.* (2011). ERG status is unrelated to PSA recurrence in radically operated prostate cancer in the absence of antihormonal therapy. Clin Cancer Res *17*, 5878-5888.

Minner, S., Jessen, B., Stiedenroth, L., Burandt, E., Kollermann, J., Mirlacher, M., Erbersdobler, A., Eichelberg, C., Fisch, M., Brummendorf, T.H., *et al.* (2010). Low level HER2 overexpression is associated with rapid tumor cell proliferation and poor prognosis in prostate cancer. Clin Cancer Res *16*, 1553-1560.

Piccolo, S.R., Sun, Y., Campbell, J.D., Lenburg, M.E., Bild, A.H., and Johnson, W.E. (2012). A single-sample microarray normalization method to facilitate personalized-medicine workflows. Genomics *100*, 337-344.

Ross, A.E., Johnson, M.H., Yousefi, K., Davicioni, E., Netto, G.J., Marchionni, L., Fedor, H.L., Glavaris, S., Choeurng, V., Buerki, C., *et al.* (2015). Tissue-based Genomics Augments Post-

prostatectomy Risk Stratification in a Natural History Cohort of Intermediate- and High-Risk Men. European urology.
Schlomm, T., Sultmann, H., and Kollermann, J. (2008). [Identification and validation of clinically relevant molecular alterations in prostate cancer]. Der Urologe Ausg A *47*, 1193-1198.
Sharma, N.L., Massie, C.E., Ramos-Montoya, A., Zecchini, V., Scott, H.E., Lamb, A.D., Macarthur, S., Stark, R., Warren, A.Y., Mills, I.G., *et al.* (2013). The androgen receptor induces a distinct transcriptional program in castration-resistant prostate cancer in man. Cancer Cell *23*, 35-47.
Subramanian, A., Tamayo, P., Mootha, V.K., Mukherjee, S., Ebert, B.L., Gillette, M.A., Paulovich, A., Pomeroy, S.L., Golub, T.R., Lander, E.S., *et al.* (2005). Gene set enrichment analysis: a knowledge-based approach for interpreting genome-wide expression profiles. Proceedings of the National Academy of Sciences of the United States of America *102*, 15545-15550.
Urbanucci, A., Sahu, B., Seppala, J., Larjo, A., Latonen, L.M., Waltering, K.K., Tammela, T.L., Vessella, R.L., Lahdesmaki, H., Janne, O.A., *et al.* (2012). Overexpression of androgen receptor enhances the binding of the receptor to the chromatin in prostate cancer. Oncogene *31*, 2153-2163.
Urbanucci, A., Waltering, K.K., Suikki, H.E., Helenius, M.A., and Visakorpi, T. (2008). Androgen regulation of the androgen receptor coregulators. BMC Cancer *8*, 219.
Waltering, K.K., Helenius, M.A., Sahu, B., Manni, V., Linja, M.J., Janne, O.A., and Visakorpi, T. (2009). Increased expression of androgen receptor sensitizes prostate cancer cells to low levels of androgens. Cancer research *69*, 8141-8149.
Ylipaa, A., Kivinummi, K., Kohvakka, A., Annala, M., Latonen, L., Scaravilli, M., Kartasalo, K., Leppanen, S.P., Karakurt, S., Seppala, J., *et al.* (2015). Transcriptome sequencing reveals PCAT5 as a novel ERG-regulated long non-coding RNA in prostate cancer. Cancer Res.
Yu, J., Yu, J., Mani, R.-S., Cao, Q., Brenner, C.J., Cao, X., Wang, X., Wu, L., Li, J., Hu, M., *et al.* (2010). An integrated network of androgen receptor, polycomb, and TMPRSS2-ERG gene fusions in prostate cancer progression. Cancer Cell *17*, 443-454.
Zhang, Y., Liu, T., Meyer, C., Eeckhoute, J., Johnson, D., Bernstein, B., Nusbaum, C., Myers, R., Brown, M., Li, W., *et al.* (2008). Model-based Analysis of ChIP-Seq (MACS). Genome biology *9*, R137.